CHEMISTRY
A EUROPEAN JOURNAL

DOI: 10.1002/chem.200701914

Luminescent Alkynylplatinum(II) Complexes of 2,6-Bis(*N*-alkylbenzimidazol-2′-yl)pyridine-Type Ligands with Ready Tunability of the Nature of the Emissive States by Solvent and Electronic Property Modulation

Anthony Yiu-Yan Tam,[a] Wai Han Lam,[a] Keith Man-Chung Wong,[a] Nianyong Zhu,[a] and Vivian Wing-Wah Yam*[a, b]

Abstract: A new class of luminescent alkynylplatinum(II) complexes of tridentate bis(*N*-alkylbenzimidazol-2′-yl)-pyridines (bzimpy), [Pt(R,R′-bzimpy)-(C≡C−R″)]X (X = PF_6, OTf), and one of their chloro precursor complexes, [Pt(R,R′-bzimpy)Cl]PF_6, have been synthesized and characterized; one of the alkynyl complexes has also been structurally characterized by X-ray crystallography. Electrochemical studies showed that the oxidation wave is alkynyl ligand-based in nature with some mixing of the metal center-based contribution, whereas the two quasi-reversible reduction couples are mainly bzimpy-based reductions. The electronic absorption and luminescence properties of the complexes have also been investigated. In solution, the high-energy and intense absorption bands are assigned as the π–π* intraligand (IL) transitions of the bzimpy and alkynyl ligands, whereas the low-energy and moderately intense absorptions are assigned to an admixture of metal-to-ligand charge-transfer (MLCT) (dπ(Pt)→π*(R,R′-bzimpy)) and ligand-to-ligand charge-transfer (LLCT) (π-(C≡C−R″)→π*(R,R′-bzimpy)) transitions. Upon variation of the electronic effects of the arylalkynyl ligands, vibronic-structured or structureless emission bands, originating from triplet metal-perturbed intraligand (IL) or an admixture of triplet metal-to-ligand charge-transfer (MLCT) and ligand-to-ligand charge-transfer (LLCT) excited states respectively, were observed in solution. Interestingly, two of the complexes showed a dual luminescence that was sensitive to the polarity of the solvents. Upon cooling from 298 K to 155 K, drastic color, UV/Vis, and luminescence changes were observed in a butyronitrile solution of **1**, and were ascribed to the formation of aggregate species through Pt···Pt and π–π stacking interactions. DFT and time-dependent DFT (TD-DFT) calculations have been performed to verify and elucidate the results of the electrochemical and photophysical properties.

Keywords: alkynyl ligands · computer chemistry · density functional calculations · N ligands · photoluminescence · platinum

Introduction

The spectroscopic and photophysical behavior of square-planar platinum(II) complexes has been extensively studied in the past few decades, due to their intriguing spectroscopic and luminescence properties.[1–9] The platinum(II) terpyridyl complexes have attracted much attention in recent years due to their propensity to exhibit Pt···Pt and π–π stacking

[a] A. Y.-Y. Tam, Dr. W. H. Lam, Dr. K. M.-C. Wong, Dr. N. Zhu, Prof. Dr. V. W.-W. Yam
Centre for Carbon-Rich Molecular and Nano-Scale Metal-Based Materials Research
Department of Chemistry and HKU-CAS Joint Laboratory of New Materials, The University of Hong Kong
Pokfulam Road, Hong Kong (P.R. China)
Fax: (+852) 2857-1586
E-mail: wwyam@hku.hk

[b] Prof. Dr. V. W.-W. Yam
State Key Laboratory of Supramolecular Structure and Materials, Jilin University
Changchun 130012 (P.R. China)

Supporting information for this article is available on the WWW under http://www.chemeurj.org/ or from the author. It contains selected structural parameters of **1′**–**8′**; TD-DFT/CPCM (CH_2Cl_2) excitation energies of selected singlet excited states; percentage composition of selected molecular orbitals; Cartesian coordinates; concentration-dependent electronic absorption and emission spectra of **2**; concentration-dependent emission spectra of a butyronitrile glass of **2** at 77 K; solid-state emission spectra of **7**; time-resolved emission spectrum of **2** and its corresponding steady-state emission spectrum; experimental UV/Vis absorption spectra of **1** and **2**, together with the calculated nonequilibrium TD-PBE1PBE/CPCM (CH_2Cl_2) singlet–singlet transitions and oscillator strengths in **1′** and **2′**; and structures and isocontour plots of the spin density of the optimized ^{3}IL/^{3}MLCT and ^{3}LLCT/^{3}MLCT excited states in **1′** and **2′**, respectively.

interactions.[3a–c,g,j,4b–c,5a–g,6f] One particular complex, $[PtCl(tpy)]^+$ (tpy = terpyridine) shows strong luminescence in the solid state.[3a–c] However, it is found to be nonemissive in fluid solution because the emissive excited state is quenched by efficient radiationless decay via a low-lying triplet ligand-field (LF) state.[3a,c,d,f,4]

Recently, our group initiated the first synthesis and isolation of a new class of alkynylplatinum(II) terpyridyl complexes.[5a] This class of compounds was luminescent in fluid solution at room temperature due to the fact that the strong field alkynyl ligand caused a larger d–d LF splitting, thereby reducing the nonradiative deactivation via the d-d LF state. In addition, this class of compounds showed much improved solubility in solution and drastic changes in spectroscopic and luminescence properties upon a change in the microenvironment and in the presence of external stimuli, such as a change in the solvent composition,[5b–c] counteranion,[5c,g] polymer,[5d] ion binding,[6a–c] pH,[6c–e] and biomolecule interactions.[5f,6g] Extension of the work to systems with molecular "sticky ends"[5e] and metallogel formation,[5g] involving interesting color changes through aggregation or degradation processes, has also been made.

Despite extensive studies on complexes with terpyridine as the tridentate ligand, a new class of tridentate N-donor ligand, 2,6-bis(benzimidazol-2′-yl)pyridine (bzimpy), has been investigated in transition metal complexes in the past two decades,[8,10–13] including Ru^{II},[10] Cu^{I},[11] Fe^{II}[12] and Ir^{III}.[13] Unlike terpyridine, bzimpy can be easily functionalized at the nitrogen atom of the benzimidazole group in the presence of strong bases, such as sodium hydride, to achieve different applications. For example, Haga et al. reported the functionalization of ruthenium(II) bzimpy complexes with disulfide groups, which were found to self-assemble on a gold surface for the fabrication of highly organized stable monolayers, thereby allowing the investigation of their electron-transfer kinetics.[10b]

Recently, $[Pt(bzimpy)Cl]^+$ derivatives were synthesized, and their aggregation[8a–c] and FRET[8d] properties were investigated. In contrast to $[PtCl(tpy)]^+$, triplet intraligand (IL) π–π* emission of the bzimpy ligand, which is lower-lying in energy than the terpyridine counterpart, was observed in solution at room temperature in $[Pt(bzimpy)Cl]^+$.[8a] This information, together with the lack of reports on alkynylplatinum(II) bzimpy complexes, have prompted us to explore this class of compounds and to investigate the nature of their electrochemical and photophysical properties. Moreover, the relative ease and versatility of synthetic modifications of both the alkynyl and bzimpy ligands may offer new opportunities for the preparation of new classes of alkynylplatinum(II) bzimpy complexes with multifunctional properties.

Herein we report the first synthesis of a new class of alkynylplatinum(II) complexes with the use of 2,6-bis(benzimidazol-2′-yl)pyridine as the tridentate N-donor ligand, [Pt(R,R′-bzimpy)(C≡CR″)]X (Scheme 1), and one of their

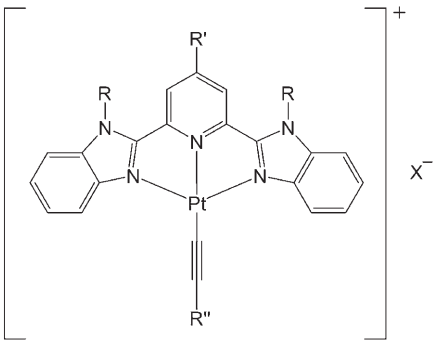

R = $C_{12}H_{25}$, R' = H, X = PF_6
2: R'' = C_6H_5
3: R'' = C_6H_4-(4-CF_3)
4: R'' = C_6H_4-(4-CH_3)
5: R'' = C_6H_4-(4-OCH_3)
6: R'' = C_6H_4-(4-NMe_2)
7: R'' = C_6H_{13}

R = $C_{12}H_{25}$, R' = $OC_{12}H_{25}$, X = PF_6
8: R'' = C_6H_5

R = C_4H_7, R' = H
9: R'' = C_6H_5, X = PF_6
10: R'' = C_6H_2-(3,4,5-$(OCH_3)_3$), X = OTf

Scheme 1. Structures of the alkynylplatinum(II) bzimpy complexes **2**–**10**.

chloro precursor complexes, $[Pt(R,R'\text{-bzimpy})Cl]PF_6$ (R = $C_{12}H_{25}$, R′ = H) (**1**). The X-ray crystal structure of **10** has been determined. The electrochemical, electronic absorption and luminescence behavior of complexes **1**–**10** have been studied. Their aggregation properties in solution have also been investigated by using variable-temperature and concentration-dependent UV/Vis and luminescence spectroscopy. Interesting luminescence properties of this class of alkynylplatinum(II) complexes in solution have been observed at ambient temperature, in which dual luminescence attributed to triplet IL (typical of the chloroplatinum(II) species) and an admixture of triplet metal-to-ligand charge-transfer (MLCT) (dπ(Pt)→π*(bzimpy)) and ligand-to-ligand charge-transfer (LLCT) (π(C≡C)→π*(bzimpy)) excited states have been observed in some cases. Simple modifications of the electronic properties of the ligands and changes in the solvent polarity were expected to perturb the relative energies of the excited states given the sensitivity of the CT state to the electronic properties of the alkynyl ligands and the solvents as well as the closeness of the energies of the IL and the CT states, leading to the ready tunability of the nature of the emissive states. Such behavior, which could not be observed in the related platinum(II) terpyridyl alkynyl complexes, is unique to this class of compounds, in which the bzimpy ligand π–π* energy is expected to be lower-lying. DFT and time-dependent DFT (TD-DFT) calculations have also been performed to elucidate the electronic structures and provide a further insight into the spectroscopic origins of this class of complexes.

Results and Discussion

Synthesis and characterization: Alkynylplatinum(II) complexes (**2**–**10**) were synthesized by the reaction of the chlor-

oplatinum(II) precursors with the corresponding alkynes in the presence of a catalytic amount of copper(I) iodide and triethylamine in dichloromethane or dimethylformamide. The complexes with $R = C_{12}H_{25}$ were purified by column chromatography on silica gel by using dichloromethane/acetone as the eluent and subsequent recrystallization by the slow diffusion of diethyl ether into dichloromethane solutions of the complexes. For the complexes with $R = C_4H_9$, column chromatography was not necessary and the products were purified simply by recrystallization by the slow diffusion of diethyl ether into an acetonitrile solution. The identities of all the newly synthesized alkynylplatinum(II) complexes have been confirmed by ^{1}H NMR spectroscopy, FAB-mass spectrometry, IR spectroscopy, and satisfactory elemental analyses. Complex **10** has also been characterized structurally by X-ray crystallography.

X-ray crystal structures: The crystal structure of the complex cation of **10** is depicted in Figure 1. Similar to the case in platinum(II) terpyridyl complexes,[3a–g,4b,5a–c,h,6b–d,f,g,9b] the

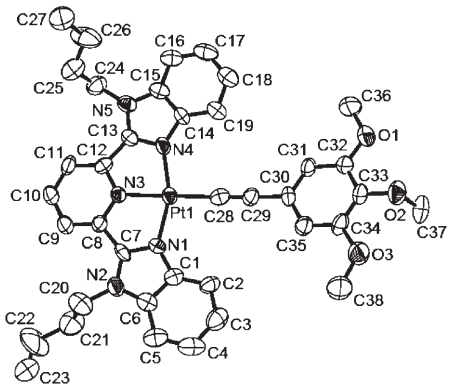

Figure 1. Perspective drawing of the complex cation of **10** with atomic numbering. Hydrogen atoms, counter-anions, and solvent molecules are omitted for clarity. Thermal ellipsoids were shown at the 30% probability level.

platinum(II) metal center adopts a distorted square-planar geometry. The N-Pt-N angles (N3-Pt1-N1 79.9°; N4-Pt1-N3 79.5°; N4-Pt1-N1 159.2°) were found to deviate from the idealized values of 90 and 180° due to the steric demand of the bzimpy ligand. The bond lengths of Pt–C and C≡C are 1.94 and 1.20 Å, respectively, which are comparable to those found in the related alkynylplatinum(II) terpyridyl complexes.[5a–c,g,6b–d,f,g] Selected bond lengths and angles are given in Table 1. The interplanar angle between the plane of the aryl ring of the arylalkynyl ligand and that of the platinum-bzimpy unit is 14.0°. The crystal packing of **10** shows a twisted head-to-tail stacking between pairs of complex cations (Figure 2a), as revealed by the individual molecules rotated with respect to their neighbors, with a C-Pt-Pt-C torsion angle of 147.9°. The complex also forms a dimeric structure arranged in a zigzag fashion (Figure 2b) with alternating "short" and "long" Pt···Pt distances of 3.38 and 5.27 Å respectively. The interplanar distance of the dimeric structure is 3.43 Å, calculated from the average distances of the atoms on the two least-squares planes. These are suggestive of an intermolecular Pt···Pt interaction between the two metal centers within the dimeric structure.[5a–c] The two [Pt(bzimpy)] coordination planes are essentially parallel and eclipsed, as revealed by the interplanar angle of 0.90° within the dimeric structure.

Table 1. Selected bond lengths [Å] and angles [°] for **10** with estimated standard deviations in parentheses.

Pt1–N1	2.01(8)	Pt1–C28	1.94(11)
Pt1–N3	1.99(7)	C28–C29	1.20(11)
Pt1–N4	2.01(7)	Pt1···Pt1	3.39(9)
N3-Pt1-N1	79.9(4)	N3-Pt1-C28	178.2(3)
N4-Pt1-N3	79.5(3)	N1-Pt1-C28	99.9(4)
N4-Pt1-N1	159.2(3)	C29-C28-Pt1	176.2(8)

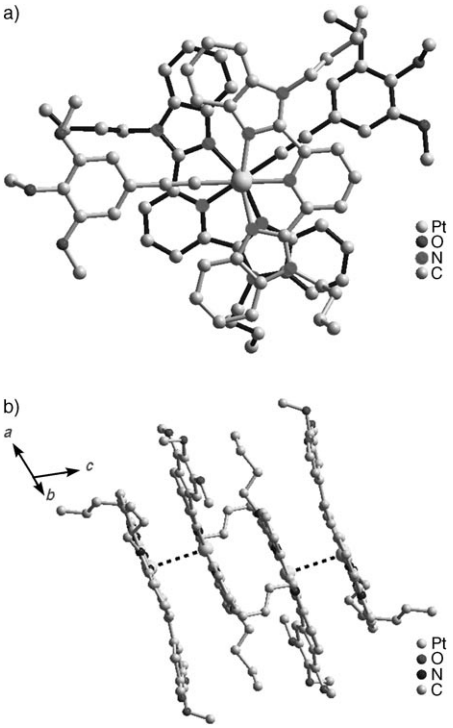

Figure 2. Crystal packing diagrams of complex cations **10** showing a) the twisted head-to-tail configuration and b) the dimeric structure in zig-zag fashion with alternating "short" and "long" Pt···Pt distances.

Electrochemistry: The cyclic voltammograms of complexes **1**–**10** in dichloromethane or dimethylformamide solutions (0.1 M nBu$_4$NPF$_6$) displayed two quasi-reversible couples at approximately −0.84 to −1.65 V and an irreversible anodic wave at approximately +0.57 to +1.68 V versus SCE. The electrochemical data for complexes **1**–**10** are summarized in Table 2, and the cyclic voltammogram of **2** in DMF (0.1 M nBu$_4$NPF$_6$) is shown in Figure 3. As the reduction potentials are found to be insensitive to the nature of the alkynyl li-

Table 2. Electrochemical data for **1**–**10**.

Complex	Oxidation E_{pa} [V] versus SCE[a]	Reduction $E_{1/2}$ [V] versus SCE[b]
1	–[c]	−0.85[d] −0.97[d]
2	+1.44[d] (+1.29[e])	−0.89[d] (−0.95[e]) −1.02[d] (−1.63[e])
3	+1.68[d]	−0.84[d] −0.99[d]
4	+1.36[d]	−0.85[d] −1.06[d]
5	+1.14[d]	−0.90[d] −1.04[d]
6	+0.57[d]	−0.95[d] −1.08[d]
7	+1.65[d]	−0.91[d] −1.07[d]
8	+1.43[d]	−1.05[d] −1.19[d]
9	+1.27[e]	−0.95[e] −1.64[e]
10	+1.17[e]	−0.93[e] −1.65[e]

[a] E_{pa} refers to the anodic peak potential for the irreversible oxidation waves. [b] $E_{1/2}=(E_{pa}+E_{pc})/2$; E_{pa} and E_{pc} are the anodic peak and cathodic peak potentials, respectively. [c] No oxidation wave was observed within the solvent window. [d] Conducted in dichloromethane solution with nBu$_4$NPF$_6$ (0.1 M; TBAH) as the supporting electrolyte at room temperature; scan rate 100 mV s^{-1}. [e] Conducted in dimethylformamide solution with nBu$_4$NPF$_6$ (0.1 M; TBAH) as the supporting electrolyte at room temperature; scan rate = 100 mV s^{-1}

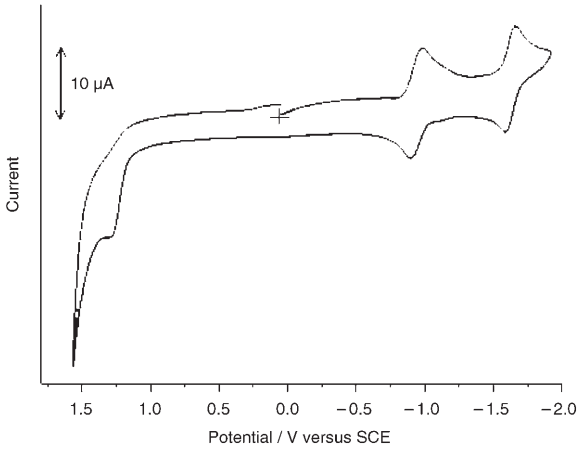

Figure 3. Cyclic voltammogram of **2** in DMF (0.1 M nBu$_4$NPF$_6$).

gands with different substituents on the phenyl ring and sensitive to the substituents at the 4-position of the bzimpy ligand, it is suggested that these couples arise from the bzimpy-based reductions that are mainly localized on the pyridine moiety. Such assignments are in line with the observation that **8** shows a more negative reduction potential than **2** because the electron-donating alkoxy substituent on the bzimpy ligand would raise the π*(bzimpy) orbital energy. This has also been supported by DFT calculations, in which the LUMO is found to be mainly derived from the π* orbital localized on the pyridine unit (vide infra).

In view of the observed change of the potentials for oxidation upon varying R″, the oxidation is attributed to alkynyl-based ligand oxidation, mixed with some metal-centered contribution.[5a,c,h,6c,h] For complexes **2**–**6** in dichloromethane solution, the ease of oxidation shows a trend of **6** (+0.57 V) > **5** (+1.14 V) > **4** (+1.36 V) > **2** (+1.44 V) > **3** (+1.68 V), in line with the order of the electron-donating ability of the alkynyl ligands, $NMe_2 > OMe > CH_3 > H > CF_3$, which would render the dπ(Pt) and π(C≡C−R″) orbitals higher-lying in energy, thus causing a shift of the potential to less anodic values. In addition, **7**, which contains an alkyl-alkynyl ligand, has been shown to display a more positive potential for this oxidation relative to **2** in dichloromethane solutions due to the fact that the decrease in π-donating ability of the alkylalkynyl ligand relative to the arylalkynyl ligand causes a lowering in the dπ(Pt) and π(C≡C−R″) orbital energies. No oxidation wave was observed in the dichloromethane solution of **1** within the solvent window (from +2.0 to −2.0 versus SCE). This suggests that the strong-field alkynyl ligand in alkynylplatinum(II) complexes destabilizes the dπ(Pt) orbital to a larger extent relative to that of the chloro derivative in **1**, which leads to the more positive oxidation potential for **1**.

Electronic absorption spectroscopy: The electronic absorption spectra of complexes **2**–**10** in solution at 298 K showed intense absorption bands at 312–384 nm and moderately intense bands at 434–584 nm. The photophysical data of **1**–**10** are summarized in Table 3. With reference to previous spectroscopic studies on alkynylplatinum(II) terpyridyl complexes[5–7,9] and the related [Pt(bzimpy)Cl]$^+$ complex,[8] the high-energy intense absorption band is assigned to the intraligand (IL) (π→π*) transitions of the alkynyl and bzimpy ligands, whereas the low-energy absorption band is tentatively assigned to an admixture of metal-to-ligand charge-transfer (MLCT) (dπ(Pt)→π*(R,R′-bzimpy)) and ligand-to-ligand charge-transfer (LLCT) (π(C≡C−R″)→π*(R,R′-bzimpy)) transitions. Complex **1** exhibited a similar UV/Vis absorption pattern, with the exception that the MLCT shoulder showed a blue shift in energy, attributed to the lack of the strong field alkynyl ligand in **1**. The electronic absorption spectra of **1**–**3**, **6**, and **8** are shown in Figure 4. For complexes **2**–**6** and **8** in dichloromethane solutions, the low-energy absorption band shows an energy trend of **8** (440 nm) > **3** (446 nm) > **2** (458 nm) > **4** (465 nm) > **5** (488 nm) > **6** (584 nm), which is in line with the charge-transfer (CT) assignment since electron-donating substituents on the phenyl ring of the alkynyl ligand would raise the energy of the dπ(Pt) and π(C≡C−R″) orbitals and result in a lowering of the CT energy,[5a,c,h] whereas the poorer π-accepting ability of 4-$C_{12}H_{25}$O-bzimpy relative to bzimpy would render the π*(4-$C_{12}H_{25}$O-bzimpy) orbital higher-lying in energy, which results in a higher CT energy.[5c] Relative to **2**, the electronic absorption spectrum of **7** showed a blue shift in the CT energy in solution, which can be explained by the greater extent of conjugation provided by the arylalkynyl ligand in **2** that results in a lowering of the transition energy.

Electronic absorption studies of **2** and **4** in dichloromethane, acetonitrile, and dimethylformamide solutions were performed to investigate solvent effect. Upon increasing the polarity of the solvents, the CT absorption band showed a blue shift in energy. As with other Pt^{II} polypyridine complexes,[6d,7a,9] negative solvatochromism was observed for the low-energy absorption band, which is in line with the expected decrease in dipole moment on going from the ground state to the excited state. Complexes **2** and **9** in

Table 3. Photophysical data for **1**–**10**.

Complex	Medium T [K]	Absorption	Emission	
		λ_{max} [nm] (ε_{max} [$dm^3 mol^{-1} cm^{-1}$])	λ_{em} [nm] (τ_o [μs])	φ_{em}[a]
1	CH_2Cl_2 (298)	320 (23300), 360 (22700), 384 (21050), 434 (1395)	565, 612 (3.28), 690[b] (1.25)	1.7×10^{-2}
	CH_3CN (298)	312 (25325), 342 (27205), 374 (24585), 434 (1430)	560, 605 (0.40), 690[b] (0.10)	1.2×10^{-3}
	solid (298)		705 (0.58)	
	solid (77)		720 (2.19)	
	glass[c] (77)		543, 585 (9.30), 640[d] (8.75)	
2	CH_2Cl_2 (298)	334 (24180), 364 (27630), 380 (26515), 458 (3870)	580, 625[f] (0.69), 740[b] (0.14)	2.9×10^{-2}
	CH_3CN (298)	325 (24025), 353 (25750), 367 (23615), 446 (3525)	565, 610 (0.35), 730[b] (0.15)	8.9×10^{-3}
	DMF (298)	329 (21210), 355 (23945), 370 (22160), 444 (4075)	565, 610 (1.51), –[e]	1.0×10^{-3}
	solid (298)		652 (0.41)	
	solid (77)		614 (2.27)	
	glass[c] (77)		543, 582 (8.22), 645[d] (4.90)	
3	CH_2Cl_2 (298)	332 (24315), 362 (27320), 378 (25305), 446 (2850)	570, 616 (2.66), 730[b] (<0.10)	9.6×10^{-2}
	CH_3CN (298)	326 (20930), 354 (23255), 372 (20100), 434 (3605)	570, 616 (0.29), 720[b] (0.21)	1.4×10^{-2}
	solid (298)		795 (1.84)	
	solid (77)		735 (2.19)	
	glass[c] (77)		540, 583 (7.60), 635[d] (5.20)	
4	CH_2Cl_2 (298)	335 (25950), 363 (29655), 381 (29100), 465 (4280)	652 (2.30), 745[b] (0.19)	2.5×10^{-3}
	CH_3CN (298)	328 (23210), 352 (25105), 372 (22315), 448 (4140)	567, 640[f] (0.29), 740[b] (0.26)	1.1×10^{-3}
	DMF (298)	326 (26570), 354 (28855), 372 (26070), 442 (5020)	567, 625[f] (3.92), –[e]	1.4×10^{-3}
	solid (298)		705 (0.71)	
	solid (77)		660 (2.04)	
	glass[c] (77)		543, 583 (9.90), 640[d] (4.75)	
5	CH_2Cl_2 (298)	336 (26465), 362 (30760), 381 (30390), 488 (4395)	565, 610 (3.20), 740[b] (0.44)	8.9×10^{-4}
	CH_3CN (298)	332 (22870), 354 (24990), 370 (23350), 460 (3990)	–[g], 740[b] (0.30)	
	solid (298)		655 (0.21)	
	solid (77)		666 (2.60)	
	glass[c] (77)		540, 580 (9.03), 642[d] (5.22)	
6	CH_2Cl_2 (298)	318 (28500), 363 (21355), 382 (20065), 584 (3960)	–[g]	
	CH_3CN (298)	306 (37830), 354 (25380), 370 (23685), 546 (4330)	–[g]	
	solid (298)		–[g]	
	solid (77)		–[g]	
	glass[c] (77)		–[g]	
7	CH_2Cl_2 (298)	330 (15560), 362 (16730), 378 (16310), 440 (2825)	575, 625 (3.55), 712[h] (0.43)	5.0×10^{-2}
	CH_3CN (298)	323 (17905), 354 (19035), 367 (17595), 436 (3925)	560, 610 (0.26), 715[h] (0.10)	9.5×10^{-3}
	solid (298)		680 (0.58)	
	solid (77)		682 (3.10)	
	glass[c] (77)		540, 580 (9.60), 648[d] (5.64)	
8	CH_2Cl_2 (298)	330 (36040), 348 (33545), 365 (29275), 440 (4990)	560, 605 (1.34), 670[b] (0.28)	8.3×10^{-2}
	solid (298)		640 (0.31)	
	solid (77)		630 (3.32)	
	glass[c] (77)		530, 570 (6.44), 610[d] (3.68)	
9	DMF (298)	329 (17875), 355 (20210), 370 (18305), 444 (3865)	565, 610 (1.36), –[e]	1.1×10^{-3}
	solid (298)		680 (0.48)	
	solid (77)		675 (2.40)	
	glass[c] (77)		545, 586 (7.86), 635[d] (5.26)	
10	DMF (298)	330 (27170), 354 (31020), 370 (29195), 450 (4660)	–[g]	
	solid (298)		660 (0.23)	
	solid (77)		670 (2.20)	
	glass[c] (77)		540, 580 (7.73), 630[d] (6.73)	

[a] The luminescence quantum yield, measured at room temperature by using $[Ru(bpy)_3]^{2+}$ as a standard. [b] Excimeric emission band observed at a concentration of $\geq 10^{-4}$ M. [c] In butyronitrile glass. [d] Aggregate emission in glassy matrix at 77 K. [e] No excimeric emission observed even at a concentration of 2×10^{-3} M. [f] Dual luminescence observed in solution at concentration $< 10^{-4}$ M at ambient temperature. [g] Nonemissive. [h] Excimeric emission band observed at a concentration of $\geq 2\times10^{-3}$ M. All solid-state emissions were recorded after grinding.

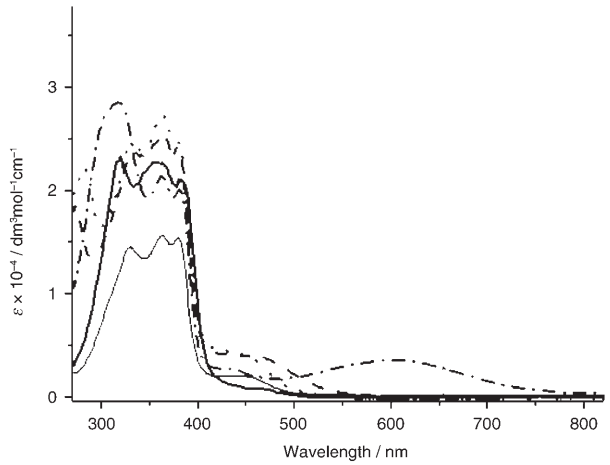

Figure 4. Electronic absorption spectra of **1** (——), **2** (– – –), **3** (•••••), **6** (–•–•), and **8** (——) in CH_2Cl_2 at room temperature.

DMF showed essentially identical UV/Vis absorption patterns with similar extinction coefficients, which suggests that no significant effect can be attributed to the chain length of the N-alkyl chains. UV/Vis absorption spectra at various concentrations of **2** in dichloromethane solution were prepared, ranging from 8.2×10^{-3} to 7.1×10^{-6} M, and the absorption tails at 550 nm were found to obey Beer's law (Figure S1, Supporting Information). This suggests the lack of any significant ground-state complex aggregation.[5a–b,6c]

As **1** in butyronitrile solution ($c=7\times10^{-4}$ M) showed a drastic color change from yellow to red upon cooling to 155 K (Figure 5), variable-temperature absorption studies were performed between 298 and 155 K. With decreasing temperature, new absorption bands at 530 and 565 nm were observed. No such absorption bands appeared at concentrations $<10^{-4}$ M, and in **2**–**10** no such bands appeared even at 77 K. The UV/Vis absorption spectra of **1** at different temperatures are shown in Figure 5. These concentration-dependent absorption bands that appeared at low temperature originated from a metal–metal-to-ligand charge-transfer (MMLCT) transition that results from an intermolecular association through Pt···Pt and π–π stacking interactions. Such MMLCT absorption bands were also observed in $[Pt(Me_2bzimpy)Cl]^+$ and were induced by vapochromic effects.[8b]

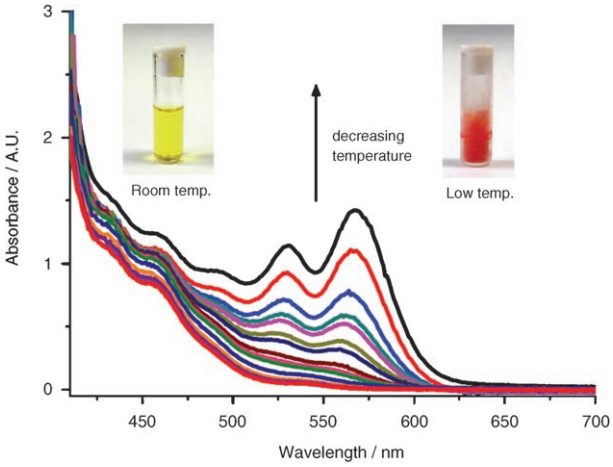

Figure 5. Electronic absorption spectra of **1** in butyronitrile solution ($c=7\times10^{-4}$ M) upon cooling from 298 to 155 K. Inset: Photographs of the butyronitrile solutions of **1** at room and low temperatures.

Luminescence spectroscopy: All of the complexes, except **5**, **6**, and **10**, which contain electron-rich OMe or NMe_2 on the arylalkynyl ligands, are strongly emissive in all states, namely in the glass state, in the solid state, and in solution. The large Stokes shifts and the long emission lifetimes, in the microsecond range, are suggestive of an origin of triplet parentage. In 77 K butyronitrile glass, all the complexes showed well-resolved vibronic-structured emission bands at approximately 530–543 nm and a low-energy emission band at approximately 630–648 nm. The vibrational progressional spacings of the high-energy band at approximately 1300 cm^{-1} are typical of the aromatic vibrational modes of the tridentate N-heterocyclic ligands. Upon excitation at $\lambda\geq$ 430 nm, the low-energy emission band increased in intensity with increasing concentrations ranging from 10^{-7} to 10^{-4} M (Figure S2, Supporting Information). The high-energy emission band is derived mainly from the triplet π–π* IL excited state of the bzimpy ligand, whereas the low-energy band, which is concentration-dependent, originated from emissive aggregates formed at low temperature.

Interestingly, the solid-state emission of this class of complexes is dependent on their morphologies.[4b] For example, whereas the yellow form of **7** showed vibronic-structured bands, the emission of the orange-red form, obtained upon grinding, became broad and structureless and was shifted to longer wavelengths (Figure S3, Supporting Information). Such a low-energy structureless emission band at approximately 652–795 nm in the solid state is assigned as a triplet MMLCT emission originating from the formation of Pt···Pt and π–π stacking interactions upon grinding.

In solution under dilute conditions ($<10^{-4}$ M) and upon excitation at $\lambda\geq$440 nm, most complexes at room temperature displayed a vibronic-structured emission band in their emission spectra with a band maximum at around 565 nm that is insensitive to the nature of the alkynyl ligands and the solvents. The vibrational progressional spacings of approximately 1300 cm^{-1} are characteristic of the vibrational stretching frequencies of the aromatic C=C and C=N modes of the tridentate N-heterocyclic ligand. This vibronic-structured emission is tentatively assigned as originating from a metal-perturbed ^{3}IL (π→π*(bzimpy)) state. The normalized emission spectra of **7** and **8** at concentrations of 2×10^{-5} M in dichloromethane are shown in Figure 6.

It is interesting to note that **2** and **4** showed unique dual luminescence behavior, which is sensitive to the nature of the solvents and substituents. Apart from the vibronic-structured emission band, **4** showed a structureless emission band with band maximum at 652 nm in dichloromethane solution, whereas in acetonitrile solution, this emission band showed a blue shift in energy (640 nm) with an additional shoulder

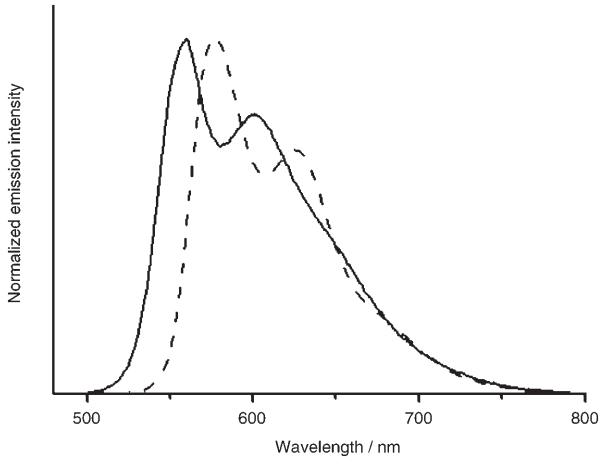

Figure 6. Normalized emission spectra of **7** (-----) and **8** (——) in degassed dichloromethane at room temperature.

at 567 nm. A further shift of this band maximum to higher energy in dimethylformamide solution (625 nm) with a slight increase in the intensity of the shoulder was observed.[9c] The emission spectra of **4** in various solvents are shown in Figure 7. Similarly, whereas **2** showed a structureless emission band at 625 nm with a shoulder at 580 nm in dichloromethane solution, a vibronic-structured emission band was observed in acetonitrile and dimethylformamide solutions.[14] The structureless emission band is unlikely to be due to excimeric or dimeric emission because it was found to be independent of concentration even down to 10^{-7} M. With reference to previous work on platinum(II) terpyridyl alkynyl complexes,[5–7] the low-energy structureless emission, the energy of which is sensitive to the nature of the substituents and solvents, originated from an admixture of ^{3}MLCT and ^{3}LLCT excited states. The high-energy band that appeared as a shoulder in the dual luminescence of **2** and **4** is believed to be derived from a triplet metal-perturbed IL origin of the bzimpy ligand; the changes in the relative energies of these two excited states would lead to the observed findings in different solvents. It is likely that upon increasing the polarity of the solvents, the CT excited state in **2** is stabilized to a lesser extent than its ground state, as expected of complexes displaying negative solvatochromism (vide supra), leading to a blue shift of the CT excited state energy. As a result, an increased chance of the occurrence of ^{3}IL emission is anticipated in more polar solvents. Similarly, this accounts for the observation of only the broad triplet CT emission band in **4** in less polar solvents, especially given the presence of the more electron-rich methyl substituent on the phenylalkynyl unit, which leads to a further lowering of the CT energy. A time-resolved emission study of **2** in dichloromethane was also performed to trace the emissions of these two origins. While emissions from both origins were observed at a gate delay of 0.25 μs, only the high-energy and longer-lived vibronic-structured emission, originating from a metal-perturbed ^{3}IL state, was observed at a gate delay of 2.25 μs (Figure S4, Supporting Information).

At concentrations $\geq 10^{-4}$ M and upon excitation at $\lambda \geq$ 480 nm, new emission bands beyond 690 nm were observed from **1–5** in dichloromethane and acetonitrile solutions, and in **8** in dichloromethane solutions at room temperature. In contrast, **7** only showed such low-energy bands at concentrations $\geq 2\times10^{-3}$ M in both solutions. This concentration-dependent and structureless emission band was suggested tentatively to be derived from excimeric or MMLCT emission at high concentrations.

Butyronitrile solutions of **1** underwent room- and low-temperature emission studies. It was found that upon excitation at $\lambda = 450$ nm, only a vibronic-structured ^{3}IL emission at 560 nm was observed at room temperature, similar to that observed in dilute solutions. Upon cooling to 155 K, a new emission band at 685 nm was observed, with a diminishment of the ^{3}IL emission band. The emission spectra of **1** in butyronitrile are shown in Figure 8. The excitation bands monitored at the low-energy emission band closely resemble the

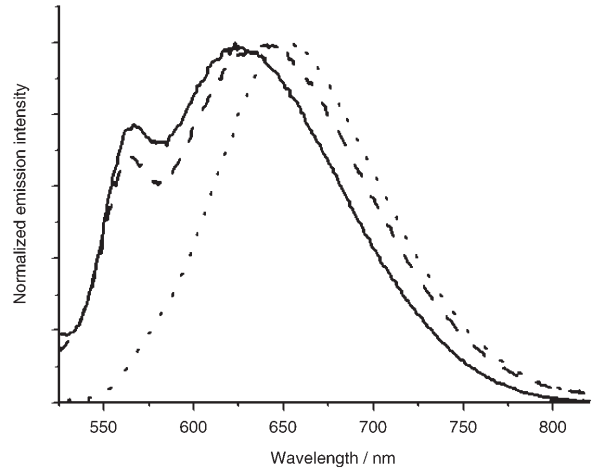

Figure 7. Emission spectra of **4** in degassed CH_2Cl_2 (•••••), CH_3CN (-----), and DMF (——) at room temperature.

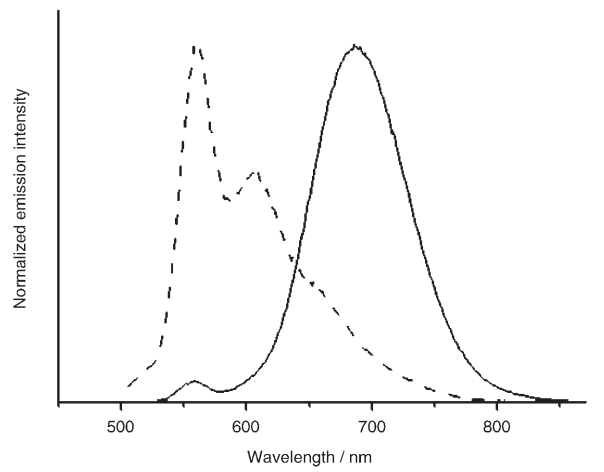

Figure 8. Emission spectra of **1** in butyronitrile solution ($c = 7\times10^{-4}$ M) at 298 (-----) and 155 K (——).

new absorption bands at 530 and 565 nm observed in the electronic absorption spectra of **1** at 155 K, which suggests that they are derived from the same origin. According to the electronic absorption studies, the new emission band probably originated from the ^{3}MMLCT excited state, which results from Pt···Pt and π–π stacking interactions formed at low temperature.

Computational studies: To gain further insight into the structural and electrochemical properties as well as the nature of absorption and emission origins of this series of platinum(II) complexes, DFT calculations at the PBE1PBE level of theory were performed to study complexes **1**–**8**. For the sake of reducing the computational cost, the long alkyl chains on the nitrogen atoms of the benzimidazolyl groups were replaced by methyl groups. In addition, the hexyl group on the alkynyl ligand was also replaced by a methyl group for complex **7**. The model complexes are labeled as **1′**–**8′**.

Geometry optimizations of the ground state for **1′**–**8′** were performed without symmetry constraint. The optimized structure of **2′** and the selected structural parameters of **1′**–**8′** are shown in Figure 9 and Table S1 (Supporting Information), respectively. For arylalkynyl complexes **2′**–**6′** and **8′**, the optimizations starting from a planar structure (with the aryl rings lying in the same plane as the [Pt(bzimpy)] plane) led to a twisted structure, in which the interplanar angles between the aryl ring of the alkynyl ligand and the [Pt(bzimpy)] plane are in the range of 31.8–90.0°, indicating that the planar structure is not a minimum in the potential energy surface. This is probably due to the steric repulsion between the hydrogen atoms at the 6,6′-positions of the two benzimidazolyl groups and those at the *ortho* positions of the aryl ring. The calculated Pt–N, Pt–C(alkynyl), and C≡C bond lengths in **2′**–**8′** are in the range of 1.993–2.015, 1.941–1.951, and 1.224–1.230 Å, respectively. Although there are no X-ray data for **1**–**8** to compare with the calculated structures of **1′**–**8′**, the calculated bond lengths and angles are comparable to those observed in the X-ray crystal structure of the analogue **10**.

The frontier molecular orbitals of complexes **1′**–**8′** obtained from TD-PBE1PBE/CPCM (CH_2Cl_2 as a solvent) were examined. For arylalkynyl and propynyl complexes **2′**–**8′**, the last three highest occupied molecular orbitals, HOMO, HOMO−1, and HOMO−2, are mainly contributed from the two orthogonal sets of π orbitals on the arylalkynyl or propynyl unit and the highest π orbital of the bzimpy ligand mixed with metal orbitals. The HOMO is composed of the antibonding interaction between the π orbitals on the C≡C triple bond and the attached aryl ring in **2′**–**6′** and **8′**, and between the π orbital on the C≡C triple bond and the C–H σ orbital from two of the three C–H bonds on the attached methyl group in **7′**. On the other hand, the first two unoccupied molecular orbitals, LUMO and LUMO+1, in **2′**–**8′** are the π* orbitals of the bzimpy ligand with a larger contribution on the pyridine unit. Figure 10 depicts the spatial plots of the frontier orbitals in **2′**. For the chloro analogue **1′**, the first two LUMOs are also the π* orbital of the bzimpy ligand, whereas the HOMO is the highest π orbital of the bzimpy ligand mixed with metal orbital, which is the same as HOMO−2 in **2′**.

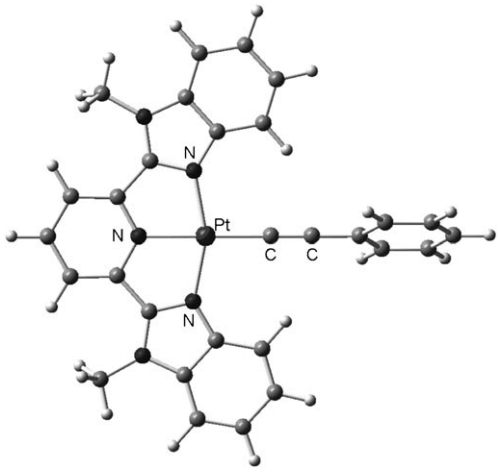

Figure 9. Optimized geometry of **2′**.

The energy level diagram of the selected frontier orbitals in complexes **2′**–**8′** is shown in Figure 11 to illustrate the effect of the substituent R″ attached to the alkynyl ligand

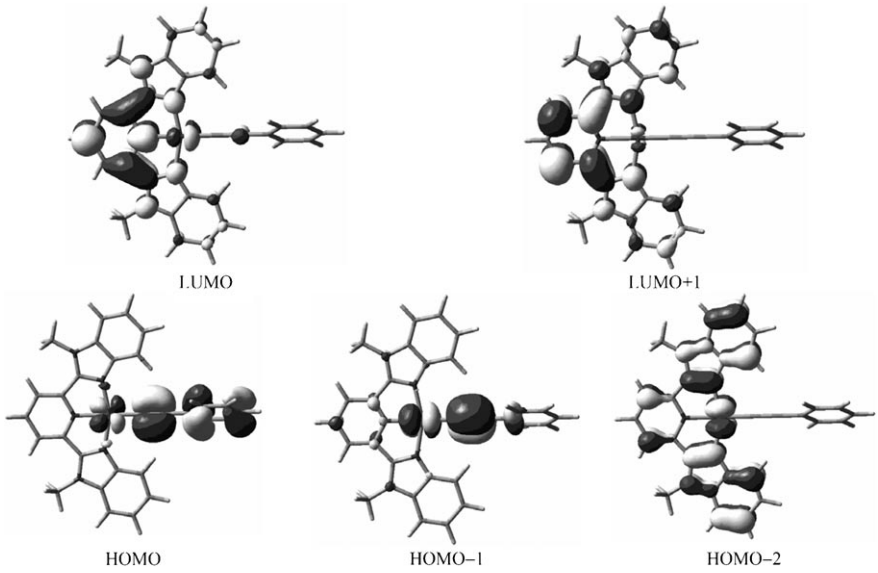

Figure 10. Spatial plots (isovalue = 0.03) of selected frontier molecular orbitals of **2′** obtained from TD-PBE1PBE/CPCM (CH_2Cl_2).

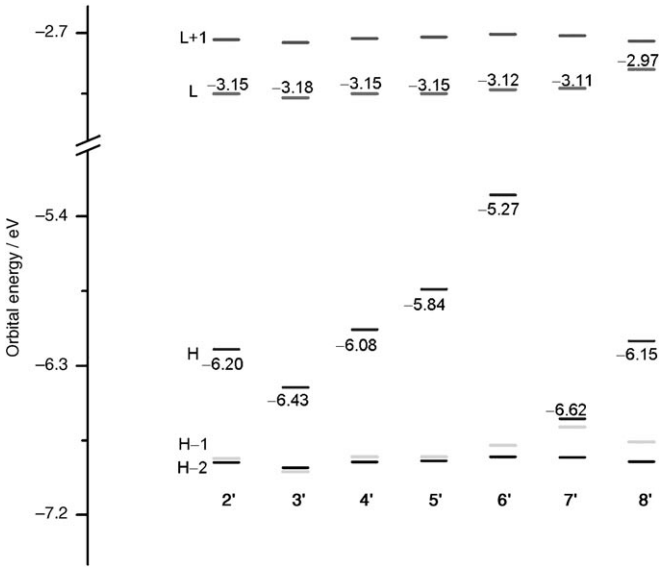

Figure 11. Orbital energy diagram of the frontier molecular orbitals in **2′** shown in Figure 10 and the corresponding orbitals in **3′**–**8′**.

on the orbital energies. As depicted, the energy of the HOMO is found to show a strong dependence on the nature of the substituents at the *para* position of the phenylalkynyl group. The HOMO energy increases in the order **3′** < **8′** ≈ **2′** < **4′** < **5′** < **6′**, which is in line with the increasing π electron-donating ability of the arylalkynyl ligand. The observed trends are consistent with the electrochemical data. The effect of the alkyl substituents attached to the alkynyl ligand on the HOMO energy is also shown in Figure 11. The HOMO energy in **7′** is decreased significantly, relative to that in **2′**. The decrease in HOMO energy is probably due to the less conjugated π system in **7′**. In contrast to the more pronounced effect of the R″ group on the HOMO energies, the LUMO energy changes very slightly with variation of the R″ group. However, the LUMO energy is increased with the π electron-donating group OMe attached to the pyridine unit of the bzimpy ligand. The calculated HOMO and LUMO in **1′**–**8′** also confirmed the assignment of the oxidation and reduction processes from the electrochemical study, respectively.

The first fifteen singlet excited states of **1′**–**8′** were calculated by using the TD-PBE1PBE/CPCM method (CH_2Cl_2 as a solvent) on the basis of the gas-phase optimized geometries. Selected low-lying transitions of **1′**–**8′** are shown in Table 4 (see Tables S2–S9 for more transitions, Supporting Information). The character of each transition is assigned

Table 4. Selected low-lying singlet excited states (S_n) in **1′**–**8′** computed by TD-PBE1PBE/CPCM (CH_2Cl_2), with the orbitals involved in the dominant excitations (H = HOMO and L = LUMO), transition coefficients, vertical excitation energies ([nm] and [eV]), oscillator strengths (*f*), and character of the excited states.

Complex	S_n	Excitation	Transition coefficient	Vertical excitation energy [nm]	[eV]	*f*[a]	Character
1′	1	H→L	0.68	457	2.71 (2.73)[b]	0.009	IL (R,R′-bzimpy→R,R′-bzimpy)[c]
2′	1	H→L	0.69	534	2.32 (2.43)[b]	0.038	LLCT (C≡CR″→R,R′-bzimpy)[c]
	2	H−2→L	0.68	454	2.73 (2.75)[b]	0.006	IL (R,R′-bzimpy→R,R′-bzimpy)[c]
	3	H→L+1	0.70	442	2.81 (2.92)[b]	0.006	LLCT (C≡C−R″→R,R′-bzimpy)[c]
	4	H−1→L	0.67	428	2.89 (2.96)[b]	0.066	LLCT (C≡C−R″→R,R′-bzimpy)[c]
3′	2	H−1→L	0.68	453	2.74 (2.76)[b]	0.007	IL (R,R′-bzimpy→R,R′-bzimpy)[c]
	3	H−2→L	0.67	419	2.96 (3.02)[b]	0.077	LLCT (C≡C−R″→R,R′-bzimpy)[c]
4′	1	H→L	0.69	551	2.25 (2.35)[b]	0.071	LLCT (C≡C−R″→R,R′-bzimpy)[c]
	2	H→L+1	0.70	457	2.71 (2.83)[b]	0.007	LLCT (C≡C−R″→R,R′-bzimpy)[c]
	3	H−2→L	0.68	454	2.73 (2.75)[b]	0.007	IL (R,R′-bzimpy→R,R′-bzimpy)[c]
	4	H−1→L	0.68	431	2.88 (2.95)[b]	0.060	LLCT (C≡C−R″→R,R′-bzimpy)[c]
5′	1	H→L	0.69	595	2.09 (2.19)[b]	0.112	LLCT (C≡C−R″→R,R′-bzimpy)
	2	H→L+1	0.70	492	2.52 (2.64)[b]	0.009	LLCT (C≡C−R″→R,R′-bzimpy)
	3	H−2→L	0.68	454	2.73 (2.75)[b]	0.006	IL (R,R′-bzimpy→R,R′-bzimpy)[c]
	4	H−1→L	0.68	433	2.86 (2.94)[b]	0.048	LLCT (C≡C−R″→R,R′-bzimpy)[c]
6′	1	H→L	0.68	741	1.67 (1.77)[b]	0.200	LLCT (C≡C−R″→R,R′-bzimpy)
	2	H→L+1	0.70	602	2.06 (2.18)[b]	0.010	LLCT (C≡C−R″→R,R′-bzimpy)
	3	H−2→L	0.68	454	2.73 (2.75)[b]	0.006	IL (R,R′-bzimpy→R,R′-bzimpy)[c]
	4	H−1→L	0.68	444	2.79 (2.87)[b]	0.032	LLCT (C≡C−R″→R,R′-bzimpy)[c]
7′	2	H−2→L	0.68	454	2.73 (2.75)[b]	0.005	IL (R,R′-bzimpy→R,R′-bzimpy)[c]
	3	H→L	0.67	449	2.76 (2.83)[b]	0.066	LLCT (C≡C−R″→R,R′-bzimpy)[c]
8′	1	H→L	0.70	504	2.46 (2.56)[b]	0.016	LLCT (C≡C−R″→R,R′-bzimpy)[c]
	2	H→L+1	0.70	451	2.75 (2.85)[b]	0.003	LLCT (C≡C−R″→R,R′-bzimpy)[c]
	3	H−2→L	0.61	424	2.92 (2.94)[b]	0.008	IL (R,R′-bzimpy→R,R′-bzimpy)[c]
	4	H−1→L	0.60	415	2.99 (3.05)[b]	0.074	LLCT (C≡C−R″→R,R′-bzimpy)[c]

[a] Only the singlet excited states with $f > 0.001$ were listed. [b] The corresponding singlet–singlet transitions computed by TD-PBE1PBE/CPCM with CH_3CN as a solvent. [c] Excited state has some MLCT character.

according to the compositions of the occupied and virtual MOs of the dominant excitation (see Table S10 for the percentage compositions of selected frontier orbitals, Supporting Information). The experimental electronic absorption spectra of **1** and **2** measured in dichloromethane together with the calculated TD-DFT/CPCM (CH_2Cl_2) transitions of complexes **1′** and **2′** are shown in Figure S5 (Supporting Information). The spectral assignment is based on the correlation of the experimental peak maxima with the calculated excited-state energies of the transitions with the oscillator strength greater than 0.001. From the calculated result of the chloro-analogue **1′** (Table S2 and Figure S5a, Supporting Information), the moderately intense low-energy absorption band corresponds to the excitation from the HOMO to LUMO, which can be assigned as an IL π–π* transition of the bzimpy ligand mixed with some MLCT (dπ(Pt)→π*(R,R′-bzimpy)) character, whereas several transitions are computed in the region of the intense high-energy absorption band, in which the most intense transition computed at 363 nm involves excitation from the next lower-energy π orbital of the bzimpy ligand (HOMO−2) to LUMO and it can be assigned as the IL π–π* transition of the bzimpy ligand.

Complex **2′** is different from complex **1′** and four transitions are computed in the region of the low-energy absorption band. These transitions consist of the combination of excitations from HOMO−2, HOMO−1 and HOMO to LUMO and LUMO+1. The lowest-energy transition corresponds to an excitation from HOMO to LUMO which can be assigned as LLCT (π(C≡C−R″)→π*(R,R′-bzimpy)) mixed with MLCT (dπ(Pt)→π*(R,R′-bzimpy)) character. The next higher transition involves an IL π–π* transition of the bzimpy ligand mixed with some MLCT (dπ(Pt)→π*(R,R′-bzimpy)) character, which is similar to the lowest-energy transition in the chloro analogue. Several transitions are computed in the high-energy absorption region. The most intense transition computed at 358 nm also consists of IL π–π* character of the bzimpy ligand.

Similar to **2′**, the low-energy absorption band in **3′**–**8′** is composed of two types of transitions, which are LLCT/MLCT (π(C≡C−R″)/dπ(Pt)→π*(R,R′-bzimpy)) and IL/MLCT (π(R,R′-bzimpy)/dπ(Pt)→π*(R,R′-bzimpy)). As shown in Table 4, the transition energy of the IL/MLCT (π(R,R′-bzimpy)/dπ(Pt)→π*(R,R′-bzimpy)) excited state does not change at all on variation of the substituent, R″, attached to the C≡C triple bond of the alkynyl ligand. However, the transition energy of the LLCT/MLCT (π(C≡C−R″)/dπ(Pt)→π*(R,R′-bzimpy)) excited state that involves HOMO→LUMO excitation is decreased with the increase of the π electron-donating ability of the aryl group in the order C_6H_5–CF_3 < C_6H_5 < C_6H_4–Me < C_6H_4–OMe < C_6H_4–NMe_2. Both transitions are blue-shifted from **2′** to **8′**. The increase in LLCT/MLCT transition energy can be explained by the π electron-donating OMe group attached to the pyridine ring in the bzimpy ligand which destabilizes the π* orbital. However, the increased gap for the IL/MLCT transition is probably due to the fact that the π* orbital, which is more localized on the pyridine unit, is destabilized to a larger extent than the π orbital of the bzimpy ligand which is more localized on the two benzimidazolyl units.

As mentioned in the previous section, negative solvatochromism for the low-energy absorption band was observed for the alkynyl complexes. To study the effect of solvent polarity on the low-lying singlet–singlet transitions, TD-DFT/CPCM calculations with CH_3CN as a solvent have also been performed for **1′**–**8′**. The computed oscillator strengths (*f*) for the transitions in CH_3CN which are not shown here are more or less the same as that in dichloromethane. However, all of the low-energy transitions in Table 4 are blue-shifted from dichloromethane to CH_3CN, in which the shift is more significant for the LLCT/MLCT (0.06–0.12 eV) than the IL/MLCT transitions (0.02 eV). Based on the calculated results in **2′**–**8′**, the red shift of the lowest energy LLCT/MLCT transitions with the increase of π-donating ability of the alkynyl ligand and blue shift of the transition energy with the increase in polarity of the solvent support the admixture of ligand-to-ligand charge-transfer and metal-to-ligand charge-transfer transitions assignment of the low-energy absorption band in **2**–**8**. In addition, although less intense, the IL/MLCT transition was found in the region of the low-energy absorption band.

Complexes **1**–**4**, **7**, and **8** showed strong phosphorescence in all the states. Two emissive states were observed in **2** and **4** upon variation of the solvent polarity whereas only one was found in the other complexes. The unrestricted Kohn–Sham approach (UPBE1PBE) was used to optimize the low-lying triplet excited states to investigate the nature of the emissive states. For complex **1′**, geometry optimization of the triplet state without symmetry constraints by starting from the ground-state structure led to an excited structure with the distortion mainly occurring in the bzimpy ligand. The optimized structure of the triplet excited state of **1′** and selected changes in the structural parameters relative to that of the ground state are shown in Figure S6 (Supporting Information). The distortion occurs mainly in one of the two benzimidazolyl units and the central pyridine ring in the bzimpy ligand, which is similar to an unsymmetric distortion for the ^{3}IL state of the related Au^{III} complexes in our previous study.[15] The lower-energy and higher-energy singly occupied molecular orbitals (SOMOs) of the triplet excited state are mainly the π orbital of the bzimpy ligand mixed with the metal orbital and the π* orbital of the bzimpy ligand, respectively, which indicates that the triplet excited state contains the IL π–π* of the bzimpy ligand with a slight mixing of MLCT character. A plot of the spin density of the ^{3}IL state reveals that the spin density is localized mainly on the bzimpy ligand with some on the metal center (Figure S7, Supporting Information). The energy of the ^{3}IL/^{3}MLCT excited state relative to the optimized ground state with the solvent correction (CH_2Cl_2) is computed at 571 nm, which compares well with the experimental emission λ_{max} (565 nm). The result further supports the metal-perturbed ^{3}IL assignment of the vibronic-structured emission band in **1**.

Geometry optimization of the triplet excited state in the alkynyl complexes **2′**–**4′**, **7′** and **8′** by starting from their cor-

responding optimized ground-state geometry resulted in an excited state containing a LLCT ($\pi(C\equiv C-R'')\rightarrow\pi^*$(R,R′-bzimpy)) mixed with MLCT character. The major structural change in the triplet excited state occurs mainly in the metal-pyridine and metal-aryl ethynyl units. The selected changes in the structural parameters and the isocontour plot of the spin density of the ^{3}LLCT/^{3}MLCT triplet excited state of **2′** are shown in Figures S6 and S7 (Supporting Information), respectively. In addition, based on the calculated triplet-excited state in **1′**, optimizations of the triplet state in **2′**–**4′**, **7′,** and **8′**, which involve populating the lowest-energy π^* orbital of the bzimpy ligand (LUMO) from the highest energy π orbital of the bzimpy ligand have also been performed. To obtain a correct set of initial guess orbitals for the optimization process, the starting geometries of **2′**–**4′**, **7′**, and **8′** were modified slightly from their corresponding ground-state structures to contain C_s symmetry, in which the aryl rings in **2′**–**4′** and **8′,** and one of the C−H bonds on the methyl group in **7′,** attached to the alkynyl ligands lie perpendicular and in the [Pt(bzimpy)] plane, respectively (the mirror plane is in the [Pt(bzimpy)] plane). For all complexes except **7′**, unsymmetric ^{3}IL/^{3}MLCT excited states that were similar to that in **1′** were found. Attempts to optimize the ^{3}IL/^{3}MLCT excited state of **7′** failed. Optimization starting with an initial guess for the ^{3}IL/^{3}MLCT excited state led to the ^{3}LLCT/^{3}MLCT excited state. Table 5 shows the relative energies of the calculated triplet excited states in **1′**–**4′**, **7′**, and **8′** together with the experimental emission maxima in dichloromethane. Based on the calculated relative energies of the triplet excited states together with the position and shape of the emission bands for the chloro and alkynyl complexes, the vibronic-structured emission in **1**, **3**, **7** and **8** is attributed to an intraligand π–π^* origin of the bzimpy ligands mixed with MLCT character. On the other hand, the dual emission bands observed in **2** and **4** are likely to originate from the lower-energy ^{3}LLCT/^{3}MLCT and higher-energy ^{3}IL/^{3}MLCT excited states.

Table 5. Relative energy of the calculated triplet excited states and experimental emission maxima for selected complexes.

	Relative energy of the calculated triplet excited states[a]		Experimental emission maximum (λ_{max}) in CH_2Cl_2 at 298 K
	^{3}LLCT/^{3}MLCT	^{3}IL/^{3}MLCT	
1′	–	571	565[b]
2′	631	562	580, 625
3′	582	563	570[b]
4′	659	561	652
7′	564	–	575[b]
8′	595	550	560[b]

[a] Energy of the optimized triplet excited states relative to the corresponding optimized ground states after a single point CPCM calculation by using CH_2Cl_2 as a solvent. [b] Vibronic-structured emission band.

Conclusion

A new class of luminescent tridentate alkynylplatinum(II) complexes has been synthesized and characterized. The X-ray crystal structure of **10** has been determined and Pt···Pt and π–π stacking interactions were found in the solid state. Electrochemical studies reveal bzimpy-based reductions and oxidations arising from the alkynyl ligands mixed with some metal character. Their electronic absorption and luminescence properties have also been investigated. In solution at room temperature, the high-energy intense absorption bands are assigned as π–π^* transitions of the bzimpy and alkynyl ligands and the low-energy moderately intense absorption bands are assigned to an admixture of metal-to-ligand charge-transfer ($d\pi(Pt)\rightarrow\pi^*$(R,R′-bzimpy)) and ligand-to-ligand charge-transfer ($\pi(C\equiv C-R'')\rightarrow\pi^*$(R,R′-bzimpy)) transitions. Variable-temperature UV/Vis spectra of **1** in butyronitrile solution showed new absorption bands upon cooling to 155 K, which is rationalized by the formation of aggregate species through Pt···Pt and π–π stacking interactions at low temperature. At room temperature, the emissive origin in solution is found to be affected by the solvent as well as the *para* substituents on the arylalkynyl ligands. In some cases, dual luminescence has been observed. The electronic structures of the ground and excited states of **1**–**8** were studied by DFT and TD-DFT calculations by using the model complexes **1′**–**8′**. For the alkynyl complexes **2′**–**8′**, the HOMO corresponds to the π orbital on the alkyl/arylalkynyl ligands with mixing of the metal orbital, whereas the LUMO consists mainly of the π^* orbital on the R,R′-bizmpy ligand. These results are in agreement with the electrochemical study. The TD-DFT/CPCM (CH_2Cl_2) calculations indicate that the lowest energy absorption band is dominated by the LLCT/MLCT ($\pi(C\equiv C-R'')/d\pi(Pt)\rightarrow\pi^*$(R,R′-bzimpy)) transition. Two triplet excited states found in **2′**–**4′** and **8′**, ^{3}LLCT/^{3}MLCT ($\pi(C\equiv C-R'')/d\pi(Pt)\rightarrow\pi^*$(R,R′-bzimpy)) and ^{3}IL/^{3}MLCT (π(R,R′-bzimpy)/$d\pi(Pt)\rightarrow\pi^*$(R,R′-bzimpy)), are possibly responsible for the dual emission in **2** and **4**, whereas the latter for the single emission in **1**, **3**, **7**, and **8**. The present work demonstrates that with the judicious choice of a strongly donating alkynyl ligand and a R,R′-bzimpy ligand, which has a low-lying IL π–π^* state, a small perturbation of the electronic properties of the ligands and the nature of the solvents could readily lead to the tuning of the nature of the emissive states as a result of the closeness of the energies of the IL and the CT excited states. Such unique behavior could not be found in the related alkynylplatinum(II) terpyridyl and $[Pt(bzimpy)Cl]^+$ complexes.

Experimental Section

Materials: Dichloro(1,5-cyclooctadiene)platinum(II) was obtained from Strem Chemicals. Sodium hydride, 1-bromobutane, 1-bromododecane, phenylacetylene, and 4-ethynyl-α,α,α-trifluorotoluene were obtained from Aldrich. (4-Methylphenyl)acetylene and (4-methoxyphenyl)acetylene were purchased from Maybridge. 1-Octyne was obtained from ABCR. 2,6-Bis(benzimidazol-2′-yl)pyridine (bzimpy),[16a] 2,6-bis(benzimidazol-2′-yl)-4-hydroxypyridine,[16b] 4-ethynyl-*N*,*N*-dimethylaniline,[17] 3,4,5-(trimethoxyphenyl)acetylene,[18] and all the N-alkylated bzimpy tridentate ligands[8a] were synthesized as described previously. The chloroplatinum(II) complex precursors were synthesized according to a modification

of literature procedures for the synthesis of chloroplatinum(II) terpyridyl complexes.[3a,e] All solvents were purified and distilled by using standard procedures before use. All other reagents were of analytical grade and were used as received.

2,6-Bis(1-dodecylbenzimidazol-2′-yl)pyridine: The compound was synthesized according to a modification of a previously reported method for the synthesis of 2,6-bis(1-octadecylbenzimidazol-2′-yl)pyridine, except that 1-bromododecane (6.2 g, 25.0 mmol) was used. 1-Bromododecane (6 mL, 25.0 mmol) was added to a solution of 2,6-bis(benzimidazol-2′-yl)pyridine (1.6 g, 5.0 mmol) and sodium hydride (oil dispersion, 60%, 1.0 g, 25.0 mmol) in DMF (20 mL). The resultant mixture was stirred overnight at 100 °C under an N_2 atmosphere. After removal of the solvents in vacuo, the residue was redissolved in $CHCl_3$, washed with water (3× 30 mL), and then dried over anhydrous Na_2SO_4. After the removal of the solvent, the residue was purified by column chromatography on silica gel (50% $CHCl_3$ in hexane) to give the pure product as a yellow oil (1.22 g, 40%). ^{1}H NMR (400 MHz, $CDCl_3$, 298 K): $\delta = 0.86$ (t, $J = 7.3$ Hz, 6H; CH_3), 1.01 (m, 36H; CH_2), 1.72 (m, 4H; CH_2), 4.69 (t, $J = 7.3$ Hz, 4H; NCH_2), 7.33 (m, 4H; benzimidazole), 7.46 (m, 2H; benzimidazole), 7.87 (m, 2H; benzimidazole), 8.04 (t, $J = 7.8$ Hz, 1H; pyridine), 8.32 ppm (d, $J = 7.8$ Hz, 2H; pyridine); positive-ion FAB MS: m/z: 649 $[M]^+$.

2,6-Bis(1-butylbenzimidazol-2′-yl)pyridine: The procedure was similar to that used to prepare 2,6-bis(1-dodecylbenzimidazol-2′-yl)pyridine, except 1-bromobutane (2.7 mL, 25.7 mmol) was used in place of 1-bromododecane. Yield: 0.9 g (67%); ^{1}H NMR (400 MHz, $CDCl_3$, 298 K): $\delta = 0.68$ (t, $J = 7.3$ Hz, 6H; CH_3), 1.06 (m, 4H; CH_2), 1.68 (m, 4H; CH_2), 4.72 (t, $J = 7.3$ Hz, 4H; NCH_2), 7.32 (m, 4H; benzimidazole), 7.46 (m, 2H; benzimidazole), 7.86 (m, 2H; benzimidazole), 8.03 (t, $J = 7.9$ Hz, 1H; pyridine), 8.32 ppm (d, $J = 7.9$ Hz, 2H; pyridine); positive-ion FAB MS: m/z: 425 $[M]^+$.

2,6-Bis(1-dodecylbenzimidazol-2′-yl)-4-dodecyloxypyridine: The procedure was similar to that used to prepare 2,6-bis(1-dodecylbenzimidazol-2′-yl)pyridine, except 2,6-bis(benzimidazol-2′-yl)-4-hydroxypyridine (0.5 g, 1.5 mmol) was used in place of 2,6-bis(benzimidazol-2′-yl)pyridine. Yield: 1.2 g (79%); ^{1}H NMR (400 MHz, $CDCl_3$, 298 K): $\delta = 0.85$ (m, 9H; CH_3), 1.06 (m, 54H; CH_2), 1.45 (m, 6H; CH_2), 4.20 (t, $J = 6.5$ Hz, 2H; OCH_2), 4.68 (t, $J = 7.3$ Hz, 4H; NCH_2), 7.32 (m, 4H; benzimidazole), 7.43 (m, 2H; benzimidazole), 7.82 (s, 2H; pyridine), 7.85 ppm (m, 2H; benzimidazole); positive-ion FAB MS: m/z: 833 $[M]^+$.

[Pt(R,R′-bzimpy)Cl]PF$_6$ (R = C$_{12}$H$_{25}$, R′ = H) (1): The complex was prepared according to a modification of a method previously reported for the synthesis of chloroplatinum(II) terpyridyl complexes.[3a,e] Yield: 0.8 g (70%); ^{1}H NMR (400 MHz, CD_3CN, 333 K): $\delta = 0.85$ (t, 6H; CH_3), 1.26 (m, 36H; CH_2), 1.76 (m, 4H; CH_2), 4.26 (t, $J = 7.3$ Hz, 4H; NCH_2), 6.96 (m, 2H; benzimidazole), 7.23 (m, 4H; benzimidazole), 7.68 (d, $J = 7.4$ Hz, 2H; benzimidazole), 8.08 (d, $J = 7.8$ Hz, 2H; pyridine), 8.62 ppm (t, $J = 7.8$ Hz, 1H; pyridine); positive-ion FAB MS: m/z: 879 $[M-PF_6]^+$; elemental analysis calcd (%) for $C_{43}H_{61}F_6N_5PClPt$: C 50.46, H 6.01, N 6.84; found: C 50.56, H 6.08, N 6.91.

[Pt(R,R′-bzimpy)Cl]OTf (R = C$_4$H$_9$, R′ = H): The procedure was similar to that used to prepare **1**, except that 2,6-bis(1-butylbenzimidazol-2′-yl)-pyridine (1.5 g, 3.5 mmol) was used in place of 2,6-bis(1-dodecylbenzimidazol-2′-yl)pyridine and the product was isolated as a trifluoromethanesulfonate salt (1.0 g, 72%). ^{1}H NMR (400 MHz, CD_3CN, 333 K): $\delta = 1.00$ (t, $J = 7.7$ Hz, 6H; CH_3), 1.49 (m, 4H; CH_2), 1.85 (m, 4H; CH_2), 4.41 (t, $J = 7.7$ Hz, 4H; NCH_2), 7.34 (m, 2H; benzimidazole), 7.47 (m, 4H; benzimidazole), 8.05 (m, 4H; benzimidazole and pyridine), 8.49 ppm (t, $J = 8.3$ Hz, 1H; pyridine); positive-ion FAB MS: m/z: 655 $[M-OTf]^+$; elemental analysis calcd (%) for $C_{28}H_{29}F_3N_5O_3SClPt\cdot H_2O$: C 40.95, H 3.81, N 8.53; found: C 41.20, H 3.72, N 8.49.

[Pt(R,R′-bzimpy)Cl]PF$_6$ (R = C$_{12}$H$_{25}$, R′ = OC$_{12}$H$_{25}$): The procedure was similar to that used to prepare **1** except that 2,6-bis(1-dodecylbenzimidazol-2′-yl)-4-dodecyloxypyridine (1.2 g, 1.4 mmol) was used in place of 2,6-bis(1-dodecylbenzimidazol-2′-yl)pyridine. Yield: 0.8 g (70%); ^{1}H NMR (400 MHz, CD_3CN, 333 K): $\delta = 0.89$ (m, 9H; CH_3), 1.26 (m, 54H; CH_2), 1.47 (m, 6H; CH_2), 4.48 (m, 6H; NCH_2, OCH_2), 7.46 (m, 4H; pyridine, benzimidazole), 7.54 (m, 4H; benzimidazole), 8.38 ppm (d, $J = 8.3$ Hz, 2H; benzimidazole); positive-ion FAB MS: m/z: 1063 $[M-PF_6]^+$; elemental analysis calcd (%) for $C_{55}H_{85}F_6N_5OClPPt\cdot 0.5(CH_2Cl_2)\cdot CH_3CN$: C 53.48, H 6.95, N 6.51; found: C 53.51, H 6.74, N 6.46.

[Pt(R,R′-bzimpy)(C≡C-C$_6$H$_5$)]PF$_6$ (R = C$_{12}$H$_{25}$, R′ = H) (2): Phenylacetylene (0.1 g, 0.6 mmol), a catalytic amount of CuI (2 mg, 5%) and NEt_3 (1 mL) were added to a degassed solution of **1** (0.2 g, 0.2 mmol) in CH_2Cl_2 (30 mL). The resultant solution was stirred at room temperature for 5 h. After removal of solvent, the residue was purified by column chromatography on silica gel by using dichloromethane/acetone 1:1 v/v as the eluent. Subsequent recrystallization by diffusion of diethyl ether into a dichloromethane solution of the product gave **2** as an orange solid (95 mg, 60%). ^{1}H NMR (400 MHz, CD_3CN, 333 K): $\delta = 0.93$ (m, 6H; CH_3), 1.30 (m, 36H; CH_2), 1.73 (m, 4H; CH_2), 4.27 (t, $J = 7.9$ Hz, 4H; NCH_2), 7.25 (d, $J = 7.3$ Hz, 2H; benzimidazole), 7.28 (m, 7H; benzimidazole; Ph), 7.49 (t, $J = 7.3$ Hz, 2H; benzimidazole), 7.81 (d, $J = 8.2$ Hz, 2H; pyridine), 8.04 ppm (m, 3H; pyridine, benzimidazole); IR (Nujol): $\tilde{\nu} = 2118$ (w; ν(C≡C)), 745 cm^{-1} (s; ν(P-F)); positive-ion FAB MS: m/z: 944 $[M-PF_6]^+$; elemental analysis calcd (%) for $C_{51}H_{66}F_6N_5PPt$: C 56.24, H 6.11, N 6.43; found: C 56.21, H 6.06, N 6.43.

[Pt(R,R′-bzimpy)(C≡CC$_6$H$_4$-(CF$_3$)-4)]PF$_6$ (R = C$_{12}$H$_{25}$, R′ = H) (3): The procedure was similar to that used to prepare complex **2**, except 4-ethynyl-α,α,α-trifluorotoluene (50 mg, 0.3 mmol) was used in place of phenylacetylene. Yield: 132 mg (78%); ^{1}H NMR (400 MHz, CD_3CN, 333 K): $\delta = 0.88$ (m, 6H; CH_3), 1.30 (m, 36H; CH_2), 1.42 (m, 4H; CH_2), 4.50 (t, $J = 7.7$ Hz, 4H; NCH_2), 7.50 (m, 6H; benzimidazole), 7.61 (d, $J = 8.1$ Hz, 2H; C_6H_4), 7.79 (d, $J = 8.1$ Hz, 2H; C_6H_4), 8.09 (d, $J = 8.3$ Hz, 2H; pyridine), 8.32 ppm (m, 3H; pyridine, benzimidazole); IR (Nujol): $\tilde{\nu} = 2114$ (w; ν(C≡C)), 753 cm^{-1} (s; ν(P-F)); positive-ion FAB MS: m/z: 1012 $[M-PF_6]^+$; elemental analysis calcd (%) for $C_{52}H_{65}F_9N_5PPt\cdot 2CH_2Cl_2$: C 52.26, H 5.55, N 5.84; found: C 52.12, H 5.94, N 5.89.

[Pt(R,R′-bzimpy)(C≡CC$_6$H$_4$-(CH$_3$)-4)]PF$_6$ (R = C$_{12}$H$_{25}$, R′ = H) (4): The procedure was similar to that used to prepare complex **2**, except (4-methylphenyl)acetylene (23 mg, 0.2 mmol) was used in place of phenylacetylene. Yield: 76 mg (54%); ^{1}H NMR (400 MHz, CD_3CN, 333 K): $\delta = 0.89$ (m, 6H; CH_3), 1.26 (m, 36H; CH_2), 1.36 (m, 4H; CH_2), 2.49 (s, 3H; CH_3), 4.29 (t, $J = 7.6$ Hz, 4H; NCH_2), 7.22 (m, 4H; C_6H_4; benzimidazole), 7.32 (m, 6H; C_6H_4; benzimidazole), 7.82 (d, $J = 8.1$ Hz, 2H; pyridine), 8.13 ppm (m, 3H; pyridine; benzimidazole); IR (Nujol): $\tilde{\nu} = 2116$ (w; $^?\nu$-(C≡C), 749 cm^{-1} (s; ν(P-F)); positive-ion FAB MS: m/z: 958 $[M-PF_6]^+$; elemental analysis calcd (%) for $C_{52}H_{68}F_6N_5PPt\cdot 2CH_2Cl_2$: C 50.95, H 5.70, N 5.50; found: C 50.46, H 5.76, N 5.69.

[Pt(R,R′-bzimpy)(C≡CC$_6$H$_4$-(OCH$_3$)-4)]PF$_6$ (R = C$_{12}$H$_{25}$, R′ = H) (5): The procedure was similar to that used to prepare complex **2**, except (4-methoxyphenyl)acetylene (60 mg, 0.5 mmol) was used in place of phenylacetylene. Yield: 176 mg (53%); ^{1}H NMR (400 MHz, CD_3CN, 333 K): $\delta = 0.89$ (m, 6H; CH_3), 1.25 (m, 36H; CH_2), 1.74 (m, 4H; CH_2), 3.94 (s, 3H; OCH_3), 4.31 (t, $J = 7.8$ Hz, 4H; NCH_2), 7.06 (d, $J = 8.7$ Hz, 2H; C_6H_4), 7.19 (m, 4H; C_6H_4, benzimidazole), 7.29 (t, $J = 7.2$ Hz, 2H; benzimidazole), 7.35 (t, $J = 7.2$ Hz, 2H; benzimidazole), 7.82 (d, $J = 8.2$ Hz, 2H; pyridine), 8.15 ppm (m, 3H; pyridine, benzimidazole); IR (Nujol): $\tilde{\nu} = 2114$ (w; ν(C≡C)), 746 cm^{-1} (s; ν(P-F)); positive-ion FAB MS: m/z: 974 $[M-PF_6]^+$; elemental analysis calcd (%) for $C_{52}H_{68}F_6N_5OPPt$: C 55.81, H 6.12, N 6.26; found: C 55.55, H 6.14, N 6.12.

[Pt(R,R′-bzimpy)(C≡CC$_6$H$_4$-(NMe$_2$)-4)]PF$_6$ (R = C$_{12}$H$_{25}$, R′ = H) (6): The procedure was similar to that used to prepare complex **2**, except 4-ethynyl-*N*,*N*-dimethylaniline (43 mg, 0.29 mmol) was used in place of phenylacetylene. Yield: 163 mg (61%); ^{1}H NMR (400 MHz, CD_3CN, 333 K): $\delta = 0.84$ (m, 6H; CH_3), 1.25 (m, 36H; CH_2), 1.69 (m, 4H; CH_2), 3.07 (s, 6H; NMe_2), 4.27 (t, $J = 8.0$ Hz, 4H; NCH_2), 6.83 (m, 4H; C_6H_4; benzimidazole), 6.98 (d, $J = 8.6$ Hz, 2H; C_6H_4), 7.13 (t, $J = 7.5$ Hz, 2H; benzimidazole), 7.28 (t, $J = 7.5$ Hz, 2H; benzimidazole), 7.65 (d, $J = 8.2$ Hz, 2H; pyridine), 8.11 ppm (m, 3H; pyridine, benzimidazole); IR (Nujol): $\tilde{\nu} = 2102$ (w; ν(C≡C)), 745 cm^{-1} (s; ν(P-F)); positive-ion FAB MS: m/z: 987 $[M-PF_6]^+$; elemental analysis calcd (%) for $C_{53}H_{71}F_6N_6PPt\cdot H_2O$: C 55.34, H 6.40, N 7.31; found: C 55.39, H 6.19, N 7.32.

[Pt(R,R′-bzimpy)(C≡C-C$_6$H$_{13}$)]PF$_6$ (R = C$_{12}$H$_{25}$, R′ = H) (7): The procedure was similar to that used to prepare complex **2**, except 1-octyne (40 mg, 0.4 mmol) was used in place of phenylacetylene. Yield: 138 mg (79%); ^{1}H NMR (400 MHz, CD_3CN, 333 K): $\delta = 0.88$ (t, 6H; CH_3 of

$NC_{12}H_{25}$), 0.95 (t, $J=7.0$ Hz, 3H; CH_3 of C_6H_{13}), 1.38 (m, 36H; CH_2 of $NC_{12}H_{25}$), 1.45 (m, 8H; 4H from CH_2 of $NC_{12}H_{25}$, 4H from CH_2 of C_6H_{13}), 1.59 (m, 2H; CH_2 of C_6H_{13}), 1.73 (m, 2H; CH_2 of C_6H_{13}), 2.83 (t, $J=7.0$ Hz, 2H; CH_2 of C_6H_{13}), 4.52 (t, $J=7.6$ Hz, 4H; NCH_2), 7.42 (t, $J=7.5$ Hz, 2H; benzimidazole), 7.49 (m, 4H; benzimidazole), 8.14 (d, $J=8.3$ Hz, 2H; pyridine), 8.45 ppm (m, 3H; pyridine, benzimidazole); IR (Nujol): $\tilde{\nu}=2020$ (w; ν(C≡C), 742 cm^{-1} (s; ν(P-F)); positive-ion FAB MS: m/z: 952 $[M-PF_6]^+$; elemental analysis calcd (%) for $C_{51}H_{74}F_6N_5PPt\cdot H_2O$: C 54.93, H 6.87, N 6.28; found: C 54.45, H 6.93, N 6.51.

Pt(R,R′-bzimpy)(C≡C-C_6H_5)]PF_6 (R=$C_{12}H_{25}$, R′=$OC_{12}H_{25}$) (8): The procedure was similar to that used to prepare complex **2**, except [Pt(R,R′-bzimpy)Cl]PF_6 (R=$C_{12}H_{25}$ and R′=$OC_{12}H_{25}$) (200 mg, 0.2 mmol) was used in place of **1**. Yield: 164 mg (78%); ^{1}H NMR (400 MHz, CD_3CN, 333 K): $\delta=0.90$ (m, 9H; CH_3), 1.32 (m, 54H; CH_2), 1.79 (m, 6H; CH_2), 3.87 (t, $J=6.7$ Hz, 2H; OCH_2), 4.28 (t, $J=7.8$ Hz, 4H; NCH_2), 7.12 (m, 4H; pyridine, benzimidazole), 7.28 (t, $J=7.9$ Hz, 2H; benzimidazole), 7.39 (m, 3H; Ph), 7.53 (m, 4H; benzimidazole, Ph), 8.43 ppm (d, $J=7.9$ Hz, 2H; benzimidazole); IR (Nujol): $\tilde{\nu}=2114$ (w; ν(C≡C)), 753 cm^{-1} (s, ν(P-F)); positive-ion FAB MS: m/z: 1128 $[M-PF_6]^+$; elemental analysis calcd (%) for $C_{63}H_{90}F_6N_5OPPt\cdot H_2O$: C 58.59, H 7.18, N 5.42; found: C 58.42, H 6.92, N 5.37.

[Pt(R,R′-bzimpy)(C≡C-C_6H_5)]PF_6 (R=C_4H_9, R′=H) (9): Phenylacetylene (60 mg, 0.6 mmol), a catalytic amount of CuI (2 mg), and NEt_3 (1 mL) were added to a degassed solution of [Pt(R,R′-bzimpy)Cl]OTf (R=C_4H_9 and R′=H) (200 mg, 0.2 mmol) in DMF (15 mL),. The resultant solution was stirred at room temperature for 5 h under a N_2 atmosphere. Upon addition of diethyl ether, the resultant mixture was stirred at room temperature for 10 min. The precipitate was filtered and washed with diethyl ether. A saturated methanolic solution of ammonium hexafluorophosphate was added to a solution of the precipitate in hot methanol. After cooling, the precipitate that formed during the metathesis reaction was filtered and washed with methanol. Subsequent recrystallization by diffusion of diethyl ether into an acetonitrile solution of the product gave **10** as an orange solid (127 mg, 79%). ^{1}H NMR (400 MHz, CD_3CN, 333 K): $\delta=0.91$ (t, $J=7.4$ Hz, 6H; CH_3), 1.37 (m, 4H; CH_2), 1.72 (m, 4H; CH_2), 4.24 (t, $J=8.0$ Hz, 4H; NCH_2), 7.36 (t, $J=7.2$ Hz, 1H; Ph), 7.40 (m, 10H; benzimidazole, Ph), 7.83 (d, $J=8.2$ Hz, 2H; pyridine), 8.10 ppm (m, 3H; pyridine, benzimidazole); IR (Nujol): $\tilde{\nu}=2120$ (w, ν(C≡C)), 753 cm^{-1} (s, ν(P-F)); positive-ion FAB MS: m/z: 719 $[M-PF_6]^+$; elemental analysis calcd (%) for $C_{35}H_{34}F_6N_5PPt$: C 48.61, H 3.96, N 8.10; found: C 48.57, H 4.04, N 8.34.

[Pt(R,R′-bzimpy)(C≡CC_6H_2-$(OCH_3)_3$-3,4,5]OTf (R=C_4H_9, R′=H) (10): The procedure was similar to that used to prepare complex **9**, except that 3,4,5-(trimethoxyphenyl)acetylene (70 mg, 0.4 mmol) was used in place of phenylacetylene. The complex was isolated as its trifluoromethanesulfonate salt and red crystals were obtained (80 mg, 45%). ^{1}H NMR (400 MHz, CD_3CN, 333 K): $\delta=0.96$ (t, $J=7.3$ Hz, 6H; CH_3), 1.50 (m, 4H; CH_2), 1.88 (m, 4H; CH_2), 3.88 (s, 3H; OCH_3), 4.00 (s, 6H; OCH_3), 4.44 (t, $J=7.5$ Hz, 4H; NCH_2), 6.64 (s, 2H; C_6H_2), 7.47 (m, 6H; benzimidazole), 8.02 (d, $J=8.2$ Hz, 2H; pyridine), 8.34 ppm (m, 3H; pyridine, benzimidazole); IR (Nujol): $\nu=2109$ (w, ν(C≡C)), 745 cm^{-1} (s, ν(P-F)); positive-ion FAB MS: m/z: 810 $[M-OTf]^+$; elemental analysis calcd (%) for $C_{39}H_{40}F_3N_5O_6SPt\cdot H_2O$: C 47.95, H 4.33, N 7.17; found: C 47.73, H 4.23, N 7.19.

Physical measurements and instrumentation: ^{1}H NMR spectra were recorded on a Bruker AVANCE 400 (400 MHz) Fourier-transform NMR spectrometer with chemical shifts reported relative to tetramethylsilane. Positive ion FAB mass spectra were recorded on a Finnigan MAT95 mass spectrometer. IR spectra were obtained as Nujol mulls on KBr disks on a Bio-Rad FTS-7 FTIR spectrometer (4000–400 cm^{-1}). Elemental analyses of the newly synthesized complexes were preformed on a Flash EA 1112 elemental analyzer at the Institute of Chemistry, Chinese Academy of Sciences.

The electronic absorption spectra were obtained by using a Hewlett–Packard 8452 A diode array spectrophotometer. The concentrations of solution samples for electronic absorption measurements were typically in the range of 2×10^{-3} to 2×10^{-5} mol dm^{-3}. Steady state excitation and emission spectra were recorded at room temperature and at 77 K on a Spex Fluorolog-3 Model FL3–211 fluorescence spectrofluorometer equipped with a R2658P PMT detector. Solid-state photophysical studies were carried out with solid samples contained in a quartz tube inside a quartz-walled Dewar flask. Measurements of the butyronitrile glass or solid-state sample at 77 K were similarly conducted with liquid nitrogen filled into the optical Dewar flask. The concentrations of complex solutions in butyronitrile for glass emission measurements were usually in the range of 10^{-6} mol dm^{-3}. All solutions for photophysical studies were degassed on a high-vacuum line in a two-compartment cell consisting of a 10 mL Pyrex bulb and a 1 cm or 4 mm path length quartz cuvette and sealed from the atmosphere by a Bibby Rotaflo HP6 Teflon stopper. The solutions were rigorously degassed with at least four successive freeze-pump-thaw cycles. Emission lifetime measurements were performed by using a conventional laser system. The concentrations of the complexes in solution for lifetime measurements were usually about 2×10^{-5} mol dm^{-3}. The excitation source used was a 355 nm output (third harmonic) of a Spectra-Physics Quanta-Ray Q-switched GCR-150–10 pulsed Nd-YAG laser. Luminescence decay signals were detected by a Hamamatsu R928 PMT and recorded on a Tektronix Model TDS-620A (500 MHz, 2GS/s) digital oscilloscope and analyzed by using a program for exponential fits. Time-resolved emission spectra were recorded on an Oriel Instruments intensified charge-coupled device (ICCD) detector (Model DH520) and were analyzed by using the InstaSpec V software. The excitation source is the same laser system as that used for lifetime measurements. The emission signal was collected by an optical fiber and dispersed onto the CCD detector with an Oriel MultiSpec 115 imaging spectrograph (Model 77480). A Stanford Research Systems (SRS) delay generator (Model DG 535) was used to produce the transistor–transistor logic (TTL) pulse needed to operate the intensifier gating electronics in the detector head. The external trigger input of the delay generator was connected to the laser's prepulse trigger output. The delay generator was controlled via an IBM AT APIB (IEEE 488) card interfaced with an IBM-compatible Pentium personal computer to allow the InstaSpec V software to send commands to control the width and delay of the TTL pulse. The system was operated at −15 °C by the single-stage system to reduce the dark current signal. Luminescence quantum yields were measured by the optical dilute method reported by Demas and Crosby.[19a] A degassed solution of $[Ru(bpy)_3]Cl_2$ in acetonitrile ($\Phi=0.062$, excitation wavelength at 436 nm) was used as the reference.[19b]

Cyclic voltammetric measurements were performed by using a CH Instruments, Inc. model CHI 620 A electrochemical analyzer. Electrochemical measurements were performed in dichloromethane or dimethylformamide solutions with 0.1 mol dm^{-3} $n$$Bu_4NPF_6$ (TBAH) as supporting the electrolyte at room temperature. The reference electrode was an Ag/$AgNO_3$ (0.1 mol dm^{-3} in acetonitrile) electrode and the working electrode was a glassy carbon electrode (CH Instruments) with a platinum wire as the counter electrode. The working electrode surface was first polished with 1 μm alumina slurry (Linde) on a microcloth (Buehler) and then with 0.3 μm alumina slurry. It was then rinsed with ultra-pure deionized water and sonicated in a beaker containing ultra-pure water for five minutes. The polishing and sonication steps were repeated twice and then the working electrode was finally rinsed under a stream of ultra-pure deionized water. The ferrocenium/ferrocene couple ($FeCp_2^{+/0}$) was used as the internal reference. All solutions for electrochemical studies were deaerated with prepurified argon gas prior to measurements.

The variable-temperature electronic absorption spectra and steady-state excitation and emission spectra were obtained by using an Oxford Instrument OptistatDN cryostat to control the working temperature in the range of 155 to 298 K.

Crystal structure determination: Single crystals of **10** suitable for X-ray diffraction studies were grown by slow diffusion of diethyl ether vapor into an acetonitrile solution of the complex. The X-ray diffraction data were collected on a MAR diffractometer with a 300 mm image plate detector by using graphite monochromatized $Mo_{K\alpha}$ radiation ($\lambda=0.71073$ Å). The images were interpreted and intensities integrated by using the DENZO program.[20] The structure was solved by direct methods employing the SHELXS-97 program.[21] Full-matrix least-squares re-

finement on F^2 was used in the structure refinement. The positions of H atoms were calculated based on riding mode with thermal parameters equal to 1.2 times that of the associated C atoms and participated in the calculation of final R indices. In the final stage of least-squares refinement, all non-hydrogen atoms were refined anisotropically. Crystallographic and structural refinement data are given in Table 6. CCDC 669783 (**10**) contains the supplementary crystallographic data for this paper. These data can be obtained free of charge from The Cambridge Crystallographic Data Centre via www.ccdc.cam.ac.uk/data_request/cif).

Computational details: Calculations were carried out by using the Gaussian 03 software package.[22] DFT at the hybrid Perdew, Burke, and Ernzerhof functional level (PBE1PBE)[23] was used to optimize the ground-state geometries of the 2,6-bis(benzimidazol-2′-yl)pyridine Pt^{II} complexes **1′–8′**. Based on the ground state optimized geometries in the gas phase, the nonequilibrium TD-DFT method[24] at the same level associated with the conductor-like polarizable continuum model (CPCM)[25] was employed to study the nature of singlet–singlet transitions in the absorption spectra of **1′–8′** (CH_2Cl_2 as the solvent). The TD-DFT/CPCM calculations have also been performed by using CH_3CN as a solvent for **1′–8′** to investigate the effect of the solvent polarity on low-lying transitions. The unrestricted UPBE1PBE was used to optimize the low-lying triplet states of all the complexes to investigate the nature of the emissive states. Single-point CPCM calculations with CH_2Cl_2 as a solvent were performed on ground and triplet excited-state optimized geometries and their relative differences were used to compare with experimental emission energies. The Stuttgart effective core potentials (ECPs) and the associated basis set were applied to describe Pt[26] with a f polarization function (ζ_f(Pt) = 0.997),[27] whereas for all other atoms, the 6-31G(d) basis set[28] was used. Vibrational frequency calculations were performed for all stationary points to verify that each was a minimum (NIMAG = 0) on the potential energy surface. No imaginary frequency was found for all the species, except the LLCT/MLCT triplet excited state of **4**, in which a very small imaginary frequency of $3.5i$ cm^{-1} was found. This excited state is considered as a minimum because the imaginary value is so small. All DFT and TD-DFT calculations were performed with a larger grid size (99590).

Table 6. Crystallographic and structural refinement data for complex **10**·1.5 CH_3CN.

empirical formula	$C_{42}H_{44.50}F_3N_{6.50}O_6PtS$
F_w	1020.49
T [K]	293(2)
λ [Å]	0.71073
crystal system	monoclinic
space group	$C2/c$
unit-cell dimensions	
a [å]	22.367(5)
b [å]	27.369(6)
c [å]	14.946(3)
β [°]	114.32(3)
V [Å^3]	8337(3)
Z	8
ρ_{calcd} [g cm^{-3}]	1.626
μ [mm^{-1}]	3.485
F(000)	4088
crystal size [mm^3]	0.4 × 0.15 × 0.1
data collection range [°]	2.45 to 25.68
index ranges	$-27 \le h \le 27$, $-33 \le k \le 33$ $-17 \le l \le 16$
no. of reflns collected	24694
no. of indep reflns	7624 (R_{int} = 0.0915)
completeness to θ [°] ([%])	25.68 (96.2)
absorp. corr.	none
refinement method	full-matrix least-squares on F^2
no. of data/ restraints/parameters	7624/25/472
Gof on F^2	0.767
final R indices[a] ($I > 2\sigma(I)$)	R_1 = 0.0464, wR_2 = 0.1007
R indices (all data)	R_1 = 0.1301, wR_2 = 0.1136
largest diff peak and hole [eÅ^{-3}]	0.905, −0.659

[a] $R_{int} = \Sigma|F_o^2 - F_o^2(\text{mean})|/\Sigma[F_o^2]$, $R_1 = \Sigma||F_o| - |F_c||/\Sigma|F_o|$ and $wR_2 = \{\Sigma[w(F_o^2 - F_c^2)^2]/\Sigma[w(F_o^2)^2]\}^{\frac{1}{2}}$.

Acknowledgements

V.W.-W.Y. acknowledges receipt of a Distinguished Research Achievement Award from the University of Hong Kong. We also acknowledge support from the URC Seed Funding for Strategic Research Theme on Organic Optoelectronics, the Faculty Development Fund of The University of Hong Kong, the RGC Central Allocation Vote (CAV) Grant (HKU 2/05C), and the National Natural Science Foundation of China and the Research Grants Council of Hong Kong Joint Research Scheme (NSFC-RGC Project No. N_HKU 737/06). A.Y.-Y.T. acknowledges the receipt of a postgraduate studentship and W.H.L. the receipt of a University Postdoctoral Fellowship from The University of Hong Kong. We also thank the Computer Center at The University of Hong Kong for providing the computational resources.

[1] a) V. M. Miskowski, V. H. Houlding, C. M. Che, Y. Wang, *Inorg. Chem.* **1993**, *32*, 2518–2524; b) W. B. Connick, D. Geiger, R. Eisenberg, *Inorg. Chem.* **1999**, *38*, 3264–3265; c) F. Hua, S. Kinayyigit, J. R. Cable, F. N. Castellano, *Inorg. Chem.* **2005**, *44*, 471–473; d) C. Ed. Whittle, J. A. Weinstein, M. W. George, K. S. Schanze, *Inorg. Chem.* **2001**, *40*, 4053–4062; e) M. Hissler, W. B. Connick, D. K. Geiger, J. E. McGarrah, D. Lipa, R. J. Lachicotte, R. Eisenberg, *Inorg. Chem.* **2000**, *39*, 447–457; f) C. M. Che, L. Y. He, C. K. Poon, T. C. W. Mak, *Inorg. Chem.* **1989**, *28*, 3081–3083; g) W. B. Connick, R. E. Marsh, W. P. Schaefer, H. B. Gray, *Inorg. Chem.* **1997**, *36*, 913–922; h) V. M. Miskowski, V. H. Houlding, *Inorg. Chem.* **1991**, *30*, 4446–4452; i) S. D. Cummings, R. Eisenberg, *J. Am. Chem. Soc.* **1996**, *118*, 1949–1960; j) V. M. Miskowski, V. H. Houlding, *Inorg. Chem.* **1989**, *28*, 1529–1533.

[2] a) W. Lu, M. C. W. Chan, N. Zhu, C. M. Che, C. Li, Z. Hui, *J. Am. Chem. Soc.* **2004**, *126*, 7639–7651; b) C. K. Koo, B. Lam, S. K. Leung, M. H. W. Lam, W. Y. Wong, *J. Am. Chem. Soc.* **2006**, *128*, 16434–16435; c) S. W. Lai, M. C. W. Chan, T. C. Cheung, S. M. Peng, C. M. Che, *Inorg. Chem.* **1999**, *38*, 4046–4055; d) V. W. W. Yam, R. P. L. Tang, K. M. C. Wong, X. X. Lu, K. K. Cheung, N. Zhu, *Chem. Eur. J.* **2002**, *8*, 4066–4076; e) W. Lu, B. X. Mi, M. C. W. Chan, Z. Hui, C. M. Che, N. Zhu, S. T. Lee, *J. Am. Chem. Soc.* **2004**, *126*, 4958–4971; f) S. C. F. Kui, I. H. T. Sham, C. C. C. Cheung, C. W. Ma, B. Yan, N. Zhu, C. M. Che, W. F. Fu, *Chem. Eur. J.* **2007**, *13*, 417–435.

[3] a) H. K. Yip, L. K. Cheng, K. K. Cheung, C. M. Che, *J. Chem. Soc. Dalton Trans.* **1993**, 2933–2938; b) R. Büchner, J. S. Field, R. J. Haines, *Inorg. Chem.* **1997**, *36*, 3952–3956; c) J. A. Bailey, M. G. Hill, R. E. Marsh, V. M. Miskowski, W. P. Schaefer, H. B. Gray, *Inorg. Chem.* **1995**, *34*, 4591–4599; d) T. K. Aldridge, E. M. Stacy, D. R. McMillin, *Inorg. Chem.* **1994**, *33*, 722–727; e) K. W. Jennette, J. T. Gill, J. A. Sadownick, S. J. Lippard, *J. Am. Chem. Soc.* **1976**, *98*, 6159–6168; f) S. W. Lai, M. C. W. Chan, K. K. Cheung, C. M. Che, *Inorg. Chem.* **1999**, *38*, 4262–4267; g) T. J. Wadas, Q. M. Wang, Y. J. Kim, C. Flaschenreim, T. N. Blanton, R. Eisenberg, *J. Am. Chem. Soc.* **2004**, *126*, 16841–16849; h) J. A. Bailey, V. M. Miskowski, H. B Gray, *Inorg. Chem.* **1993**, *32*, 369–370; i) M. G. Hill, J. A. Bailey, V. M. Miskowski, H. B. Gray, *Inorg. Chem.* **1996**, *35*, 4585–4590; j) J. Moussa, K. M. C. Wong, L. M. Chamoreau, H. Amouri, V. W. W. Yam, *Dalton Trans.* **2007**, 3526–3530.

[4] a) D. K. Crites, C. T. Cunningham, D. R. McMillin, *Inorg. Chim. Acta*, **1998**, 346–353; b) R. Büchner, C. T. Cunningham, J. S. Field, R. J. Haines, D. R. McMillin, G. C. Summerton, *J. Chem. Soc. Dalton Trans.* **1999**, 711–717; c) G. Arena, G. Calogero, S. Campa-

gna, L. M. Scolaro, V. Ricevuto, R. Romeo, *Inorg. Chem.* **1998**, *37*, 2763–2769; d) J. F. Michalec, S. A. Bejune, D. R. McMillin, *Inorg. Chem.* **2000**, *39*, 2708–2709.

[5] a) V. W. W. Yam, R. P. L. Tang, K. M. C. Wong, K. K. Cheung, *Organometallics* **2001**, *20*, 4476–4482; b) V. W. W. Yam, K. M. C. Wong, N. Zhu, *J. Am. Chem. Soc.* **2002**, *124*, 6506–6507; c) V. W. W. Yam, K. H. Y. Chan, K. M. C. Wong, N. Zhu, *Chem. Eur. J.* **2005**, *11*, 4535–4543; d) C. Yu, K. M. C. Wong, K. H. Y. Chan, V. W. W. Yam, *Angew. Chem.* **2005**, *117*, 801–804; *Angew. Chem. Int. Ed.* **2005**, *44*, 791–794; e) V. W. W. Yam, K. H. Y. Chan, K. M. C. Wong, B. W. K. Chu, *Angew. Chem.* **2006**, *118*, 6315–6319; *Angew. Chem. Int. Ed.* **2006**, *45*, 6169–6173; f) C. Yu, K. H. Y. Chan, K. M. C. Wong, V. W. W. Yam, *Proc. Natl. Acad. Sci. USA*, **2006**, *103*, 19652–19657; g) A. Y. Y. Tam, K. M. C. Wong, G. Wang, V. W. W. Yam, *Chem. Commun.* **2007**, 2028–2031; h) E. Shikhova, E. O. Danilov, S. Kinayyigit, I. E. Pomestchenko, A. D. Tregubov, F. Camerel, P. Retailleau, R. Ziessel, F. N. Castellano, *Inorg. Chem.* **2007**, *46*, 3038–3048.

[6] a) W. S. Tang, X. X. Lu, K. M. C. Wong, V. W. W. Yam, *J. Mater. Chem.* **2005**, *15*, 2714–2720; b) H. S. Lo, S. K. Yip, K. M. C. Wong, N. Zhu, V. W. W. Yam, *Organometallics* **2006**, *25*, 3537–3640; c) Q. Z. Yang, Q. X. Tong, L. Z. Wu, Z. X. Wu, L. P. Zhang, C. H. Tung, *Eur. J. Inorg. Chem.* **2004**, 1948–1954; d) K. M. C. Wong, W. S. Tang, X. X. Lu, N. Zhu, V. W. W. Yam, *Inorg. Chem.* **2005**, *44*, 1492–1498; e) X. Han, L. Z. Wu, G. Si, J. Pan, Q. Z. Yang, L. P. Zhang, C. H. Tung, *Chem. Eur. J.* **2007**, *13*, 1231–1239; f) H. S. Lo, S. K. Yip, N. Zhu, V. W. W. Yam, *Dalton Trans.* **2007**, 4386–4389; g) K. M. C. Wong, W. S. Tang, B. W. K. Chu, N. Zhu, V. W. W. Yam, *Organometallics* **2004**, *23*, 3459–3465; h) S. Chakraborty, T. J. Wadas, H. Hester, C. Flaschenreim, R. Schmehl, R. Eisenberg, *Inorg. Chem.* **2005**, *44*, 6284–6293.

[7] a) F. N. Castellano, I. E. Pomestchenko, E. Shikhova, F. Hua, M. L. Muro, N. Rajapakse, *Coord. Chem. Rev.* **2006**, *250*, 1819–1828; b) H. Yersin, D. Donges, *Top. Curr. Chem.* **2001**, *214*, 81–186; c) S. W. Lai, C. M. Che, *Top. Curr. Chem.* **2004**, *241*, 27–63.

[8] a) K. Wang, M. A. Haga, H. Monjushiro, M. Akiba, Y. Sasaki, *Inorg. Chem.* **2000**, *39*, 4022–4028; b) L. J. Grove, J. M. Rennekamp, H. Jude, W. B. Connick, *J. Am. Chem. Soc.* **2004**, *126*, 1594–1595; c) E. J. Rivera, C. Figueroa, J. L. Colón, L. Grove, W. B. Connick, *Inorg. Chem.* **2007**, *46*, 8569–8576; d) V. G. Vaidyanathan, B. U. Nair, *Eur. J. Inorg. Chem.* **2005**, 3756–3759.

[9] a) J. F. Michalec, S. A. Bejune, D. G. Cuttell, G. C. Summerton, J. A. Gertenbach, J. S. Field, R. J. Haines, D. R. McMillin, *Inorg. Chem.* **2001**, *40*, 2193–2200; b) B. C. Tzeng, W. F. Fu, C. M. Che, H. Y. Chao, K. K. Cheung, S. M. Peng, *J. Chem. Soc. Dalton Trans.* **1999**, 1017–1023; c) I. E. Pomestchenko, F. N. Castellano, *J. Phys. Chem. A* **2004**, *108*, 3485–3492.

[10] a) S. C. Yu, S. Hou, W. K. Chan, *Marcomolecules* **1999**, *32*, 5251–5256; b) M. A. Haga, H. G. Hong, Y. Shiozawa, Y. Kawata, H. Monjushiro, T. Fukuo, R. Arakawa, *Inorg. Chem.* **2000**, *39*, 4566–4573.

[11] a) C. Piguet, G. Bernardinelli, A. F. Williams, *Inorg. Chem.* **1989**, *28*, 2920–2925; b) C. Piguet, B. Bocquet, E. Müller, A. F. Williams, *Helv. Chim. Acta* **1989**, *72*, 323–337; c) S. Rüttimann, C. Piguet, G. Bernardinelli, B. Bocquet, A. F. Williams, *J. Am. Chem. Soc.* **1992**, *114*, 4230–4237.

[12] A. W. Addison, S. Burman, C. G. Wahlgren, *J. Chem. Soc. Dalton Trans.* **1987**, 2621–2630.

[13] S. Obara, M. Itabashi, F. Okuda, S. Tamaki, Y. Tanabe, Y. Ishii, K. Nozaki, M. A. Haga, *Inorg. Chem.* **2006**, *45*, 8907–8921.

[14] Luminescent impurities that may lead to dual luminescence have been ruled out given the rigour of the purification steps taken. The complexes were first purified by column chromatography, followed by recrystallization. Subsequent metathesis reactions were performed to transform the PF_6^- salt to its Cl^- salt and then back to the PF_6^- salt, with each metathesized product being copiously washed and purified. The final metathesized products were obtained by recrystallization and dual luminescence was still observed.

[15] K. M. C. Wong, L. L. Hung, W. H. Lam, N. Zhu, V. W. W. Yam, *J. Am. Chem. Soc.* **2007**, *129*, 4350–4365.

[16] a) A. W. Addison, P. J. Burke, *J. Heterocycl. Chem.* **1982**, *18*, 803–805; b) P. Froidevaux, J. M. Harrowfield, A. N. Sobolev, *Inorg. Chem.* **2000**, *39*, 4678–4687.

[17] H. Takalo, J. Kankare, E. Hänninen, *Acta Chem. Scand.* **1988**, *B42*, 448–454.

[18] O. Provot, A. Giraud, J. F. Peyrat, M. Alami, J. D. Brion, *Tetrahedron Lett.* **2005**, *46*, 8547–8550.

[19] a) J. N. Demas, G. A. Crosby, *J. Phys. Chem.* **1971**, *75*, 991–1024; b) L. Wallace, D. P. Rillema, *Inorg. Chem.* **1993**, *32*, 3836–3843.

[20] Written with the cooperation of the program authors Z. Otwinowski, W. Minor: D. Gewirth *DENZO: "The HKL Manuals-A description of programs DENZO, XDISPLAYF, and SCALEPACK"*, Yale University, New Haven, **1995**.

[21] SHELXL97, G. M. Sheldrick, *Programs for Crystal Structure Analysis (release 97–2)*; University of Göttingen, Göttingen, (Germany), **1997**.

[22] Gaussian 03 (Revision C.02), M. J. Frisch, G. W. Trucks, H. B. Schlegel, G. E. Scuseria, M. A. Robb, J. R. Cheeseman, J. A. Montgomery, Jr., T. Vreven, K. N. Kudin, J. C. Burant, J. M. Millam, S. S. Iyengar, J. Tomasi, V. Barone, B. Mennucci, M. Cossi, G. Scalmani, N. Rega, G. A. Petersson, H. Nakatsuji, M. Hada, M. Ehara, K. Toyota, R. Fukuda, J. Hasegawa, M. Ishida, T. Nakajima, Y. Honda, O. Kitao, H. Nakai, M. Klene, X. Li, J. E. Knox, H. P. Hratchian, J. B. Cross, V. Bakken, C. Adamo, J. Jaramillo, R. Gomperts, R. E. Stratmann, O. Yazyev, A. J. Austin, R. Cammi, C. Pomelli, J. W. Ochterski, P. Y. Ayala, K. Morokuma, G. A. Voth, P. Salvador, J. J. Dannenberg, V. G. Zakrzewski, S. Dapprich, A. D. Daniels, M. C. Strain, O. Farkas, D. K. Malick, A. D. Rabuck, K. Raghavachari, J. B. Foresman, J. V. Ortiz, Q. Cui, A. G. Baboul, S. Clifford, J. Cioslowski, B. B. Stefanov, G. Liu, A. Liashenko, P. Piskorz, I. Komaromi, R. L. Martin, D. J. Fox, T. Keith, M. A. Al-Laham, C. Y. Peng, A. Nanayakkara, M. Challacombe, P. M. W. Gill, B. Johnson, W. Chen, M. W. Wong, C. Gonzalez, J. A. Pople, Gaussian, Inc., Wallingford CT, **2004**.

[23] a) M. Ernzerhof, G. E. Scuseria *J. Chem. Phys.* **1999**, *110*, 5029–5036; b) M. Ernzerhof, J. P. Perdew, K. Burke, *Int. J. Quantum Chem.* **1997**, *64*, 285–295.

[24] a) R. E. Stratmann, G. E. Scuseria, M. J. Frisch, *J. Chem. Phys.* **1998**, *109*, 8218–8224; b) R. Bauernschmitt, R. Ahlrichs, *Chem. Phys. Lett.* **1996**, *256*, 454–464; c) M. E. Casida, C. Jamorski, K. C. Casida, D. R. Salahub, *J. Chem. Phys.* **1998**, *108*, 4439–4449.

[25] a) V. Barone, M. Cossi, *J. Phys. Chem. A* **1998**, *102*, 1995–2001; b) M. Cossi, N. Rega, G. Scalmani, V. Barone, *J. Comput. Chem.* **2003**, *24*, 669–681.

[26] D. Andrae, U. Häussermann, M. Dolg, H. Stoll, H. Preuss, *Theor. Chim. Acta* **1990**, *77*, 123–141.

[27] A. W. Ehlers, M. Böhme, S. Dapprich, A. Gobbi, A. Höllwarth, V. Jonas, K. F. Köhler, R. Stegmann, A. Veldkamp, G. Frenking, *Chem. Phys. Lett.* **1993**, *208*, 111–114.

[28] a) W. J. Hehre, R. Ditchfield, J. A. Pople, *J. Chem. Phys.* **1972**, *56*, 2257–2261; b) P. C. Hariharan, J. A. Pople, *Theor. Chim. Acta* **1973**, *28*, 213–222; c) M. M. Francl, W. J. Pietro, W. J. Hehre, J. S. Binkley, M. S. Gordon, D. J. Defrees, J. A. Pople, *J. Chem. Phys.* **1982**, *77*, 3654–3665.

Received: December 5, 2007
Published online: April 7, 2008

